공학박사 학위논문

A study on the microstructure and mechanical properties of Li-ion battery aqueous anode slurries using capillary suspensions

모세관 현탁액을 이용한 리튬 이온 배터리 수계 음극 슬러리의 내부 구조 제어 및 이를 통한 전극의 기계적 물성 개선 방안에 관한 연구

2021년 8월

서울대학교 대학원

화학생물공학부

박 지 은

A study on the microstructure and mechanical properties of Li-ion battery aqueous anode slurries using capillary suspensions

모세관 현탁액을 이용한 리튬 이온 배터리 수계 음극 슬러리의 내부 구조 제어 및 이를 통한 전극의 기계적 물성 개선 방안에 관한 연구

지도 교수 안 경 현

이 논문을 공학박사 학위논문으로 제출함
2021년 7월

서울대학교 대학원
화학생물공학부
박 지 은

박지은의 공학박사 학위논문을 인준함
2021년 7월

위 원 장 _____

부위원장 _____

위 원 _____

위 원 _____

위 원 _____

Abstract

A study on the microstructure and mechanical properties of Li-ion battery aqueous anode slurries using capillary suspensions

Jieun Park

School of Chemical and Biological Engineering

Seoul National University

The distinct structure and flow properties of capillary suspensions, i.e., ternary solid/fluid/fluid systems including two immiscible fluids, make these new slurries promising candidates for the fabrication of Li-ion battery electrodes. In this thesis, we investigate the microstructure and mechanical properties of Li-ion battery electrode prepared with capillary suspension processing.

First, we investigate how the capillary suspension processing affects the structure and flow of the wet battery paste as well as the adhesion of the dry anode layer. It is found that the distribution of SBR particles, frequently used as a binder in the graphite slurries,

is changed when the capillary suspension concept is applied. Combining rheological, interfacial and structural investigations reveals that the SBR particles are localized at the interface of both liquid phases, and the amount of added SBR and the energy input for dispersing the secondary fluid offer extra degrees of freedom for adjusting the flow properties and microstructure according to processing and product demands. Most importantly, at a given SBR content, the adhesion strength of the capillary-suspension-type graphite slurries to the current collector is substantially higher than that made from conventional slurries. This novel approach promises battery electrodes with extended durability at a low binder content and improved electrical conductivity.

Second, we control the drying characteristics and mechanical stability by applying the concept of capillary suspension to the battery slurry. The network structure formed inside the slurry using the capillary suspension processing is confirmed by the rheological properties and cryo-scanning electron microscopy (cryo-SEM) images. It is found that the pendular bridges of the secondary fluid restrict the rearrangement of particles during drying, and thus lower the residual stress of the electrodes as evidenced by the drying stress and Fourier transformation infrared (FT-IR) spectroscopy. Due to the reduction in residual stress and

porous structural features, the capillary suspension-based electrodes are more sustainable to severe deformation such as repetitive bending.

In conclusion, this thesis proposes a new method that can dramatically enhance the mechanical properties and stability of electrodes that could possibly be applied to the next-generation battery technology.

Keyword : battery slurry, capillary suspension, microstructure, particle network, adhesion properties, drying

Student Number : 2017-38662

Contents

List of Figures

List of Tables

Chapter 1.

Introduction

Chapter 1. Introduction

1.1 General introduction

The term capillary suspension refers to suspensions whose microstructure is dominated by capillary forces. Such suspensions are ternary systems consisting of two immiscible liquids, called the bulk fluid and the secondary fluid, and solid particles. The flow behavior of a suspension substantially changes when a small amount of immiscible secondary fluid is introduced due to capillary forces inducing self-assembly of a sample spanning the network structure [1, 2].

Two distinct states of capillary suspensions have been observed, the so-called pendular and capillary states. The pendular state refers to the state where the secondary fluid wets the particles better than the bulk fluid. In this case, the secondary fluid creates pendular shaped liquid bridges between particles inducing a capillary force-driven network structure in the suspension. In the capillary state, the secondary fluid wets particles less than the bulk fluid. In this case, particle clusters form around small secondary fluid droplets because these configurations are energetically favored. Then, these clusters self-assemble into a percolating

network structure [3, 4].

The characteristics of the suspension change substantially due to the network structure of the particles. Network formation suppresses sedimentation of the particles and improves the suspension stability, but it also alters the rheological properties of the suspension drastically. The addition of a secondary fluid leads to an increase in the yield stress and a low shear viscosity regardless of the state.

Due to these changes in properties, there have been many attempts to apply the concept of capillary suspensions to various industrial slurries. Capillary suspensions have also been used as pre-cursors for the fabrication of porous sintering materials with distinct porosity and pore size specifications [5]. Due to their unique flow behavior, they are ideally suited for direct ink writing (DIW) to obtain highly porous cellular ceramic parts with unique specific strengths [6]. Sedimentation stability and atomization behavior could be improved in coke slurries [7]. The film formation of titanium dioxide pastes [8] and the conductivity of nickel and silver pastes for printed electronics were improved when a secondary fluid was introduced [9]. In addition, it was used for regulating the flow properties of food suspensions [10] and adjusting the flow behavior of a polymer ternary blend [11]. Since the network structure of a

capillary suspension provides a porous structure after drying [5, 12], it was used for ceramic materials with increased porosity and enhanced shape accuracy [13].

Bitsch et al. applied the concept of capillary suspensions to Li-ion battery slurries, and they were able to improve the surface homogeneity in slot-die coating operations [14]. High capacity graphite electrodes with a superior electrochemical performance were obtained by combining a conventionally prepared anode layer adjacent to the current collectors and a capillary suspension based second layer that included the same particles and binders [15, 16].

However, this approach deteriorated the adhesion properties of the battery electrodes by 20-30 %. Adhesion between the electrode layer and current collector is decisive for the battery life time and an important cell performance features [17]. The adhesion strength is tightly related to the type and amount of binder used in the slurries [18-20]. The most common binder for aqueous battery slurries is styrene-butadiene rubber (SBR) latex [21, 22]. Therefore, we wanted to understand how the SBR-latex affects the formation and structure of graphite based capillary-suspension-type slurries that are used in the fabrication of lithium ion battery anodes. Furthermore, we wanted to elucidate how the specific structure and potential colloidal interactions with other ingredients affect the adhesion

performance of the slurries including the SBR binder.

With the recent advances in the use of lithium-ion batteries, studies on battery slurries have been increasing [23-25]. Not only the material and composition of the slurry, but also the process [26-28], internal structure [29-33], and drying process [34-36] are getting more attention. In the coating and drying process of thin films such as electrodes, film defects can occur [37]. When the slurry or particulate suspension is coated on the substrate and dried, the coating film shrinks, which develops stress inside the film and causes film defects such as crack, curl, and delamination [37, 38]. Therefore, to manufacture electrodes with stable mechanical properties, it is necessary to control the stress that occurs during drying. Schneider et al. applied capillary suspensions to various particle systems, such as TiO2 and ZnO, to suppress cracks occurring during drying [8]. They reported that the secondary fluid evaporates later than the bulk fluid, thereby maintaining the particle network structure, increasing the distribution uniformity of the particles, and inhibiting cracks as the local stress distribution becomes uniform. Fischer and Koos [39] investigated the drying mechanism of capillary suspensions with various drying conditions, and compared with pure suspension. They reported that the change in the drying pattern could suppress film defect such as trenches and pinholes [40]. However, the drying

mechanism of the capillary suspension still needs to be discussed with various material systems. Previous studies mainly focused on fatty alcohol or oil based systems where the secondary fluid is aqueous, but the aqueous system needs to be investigated too. Moreover, the changes in mechanical properties in the thin film from the capillary suspension have not yet been fully explored. To apply capillary suspension processing to industrial products, it is necessary to understand the drying mechanism and the changes of mechanical properties.

We tried to identify the drying mechanism of aqueous Li-ion battery electrode slurry, in which the capillary suspension concept was applied. We observed how the bending strength and fracture pattern of dry electrode change after modifying the microstructure of the slurry through the capillary suspension processing.

1.2 Outline of the thesis

In this thesis, we investigated the microstructure and mechanical properties of Li-ion battery electrode using capillary-suspension-type slurries. The thesis consists of introduction, background, experimental methods, results and discussion, and summary chapters.

Chapter 1 is an introduction part where the general introduction and outline is included.

Chapter 2 describes basic background of the capillary suspensions. The first part of the background describes the definition and characteristics of the capillary suspension. The second part explains the structure formation of the capillary suspension.

Chapter 3 describes experimental method used in this thesis such as sample preparation and characterization. First, preparation method of capillary suspension using Li-ion battery anode slurry materials is introduced. Then, characterization methods for liquid state and solid state are described. Flow properties and microstructure of the slurries are measured using rheological measurement and electron microscopy. The images of electron microscopy are analyzed using image processing method.

Interfacial properties are characterized using emulsion formation method and pendent drop method. After measuring properties of the slurries in a liquid state, we prepared an electrode by coating and drying of the slurries. Then, characterization methods to investigate the solid-state properties of the electrodes are introduced. Porosity measurement which can examine the microstructure of the electrode is described. Adhesion properties and bending properties which is related to durability and stability of the electrode are described. In addition, drying behavior is characterized using drying stress measurement and FT-IR.

Chapter 4 describes the results and discussion about the microstructure and mechanical properties of the capillary suspension type Li-ion battery electrodes. In the first part of the results and discussion, controlling SBR binder distribution using capillary suspension is described. SBR binder is used for adhesion enhancement of the battery electrode. The main objective of the first part is to control distribution of SBR binder and improve adhesion properties using the concept of capillary suspension. The effect of SBR binder on the rheological properties and the microstructure of the capillary suspensions with different mixing conditions are discussed. Then, the distribution of the SBR binder in the capillary suspension is discussed by measuring interfacial

properties. Adhesion characteristic is introduced to confirm the effect of capillary suspensions and changes in SBR binder distribution on the mechanical properties.

In the second part, drying behavior and mechanical properties of capillary suspension battery electrode are described. Since the effect of the capillary suspension on the adhesion properties even after drying process is verified in the first part, it is necessary to focus on the drying process and other mechanical properties. First, the effect of the secondary fluid on the rheological properties is described. Then, capillary suspension electrodes are prepared depending on the amount of the secondary fluid in the capillary suspensions. The drying stress and porosity of the electrode are introduced to characterize the properties of the solid electrode. The relationship between the liquid state microstructure and solid state microstructure is verified using structure analysis method and FT-IR. The mechanical properties such as bending properties of the electrodes is also described.

Chapter 5 summarizes the results on the studies about the microstructure and mechanical properties of the battery electrode when applying the concept of capillary suspension.

Chapter 2.

Background

Chapter 2. Background

2.1 Capillary suspension

The concept of capillary suspension was introduced in E. Koos' paper of "Capillary Forces in Suspension Rheology"[1]. When a fluid is injected between the fine particles, capillary forces are induced and the fine particles form a complex structure. Discussions on such phenomena had been around for some time, but this paper was the first to extend and systematize that concept into the suspension domain. Since then, studies on the capillary suspension have been actively investigated[3, 4, 11, 41].

Capillary suspensions are suspensions whose physical properties are adjusted by capillary forces. Capillary suspensions are ternary systems which consist of a bulk fluid, a secondary fluid and particles. The bulk fluid is the main solvent of the suspension, and the secondary fluid is the additional liquid to adjust flow properties using capillary forces. The secondary fluid is located between or around particles to form a cluster and the particle network structure.[42]

Adding a small amount of secondary fluid into to a suspension changes flow behavior substantially. The force between two

equally-sized spheres connected by a pendular bridge is given by,

$$F_c = 2\pi r \Gamma \cos\theta \quad (1)$$

where r is a radius, Γ is the surface tension and θ is the wetting angle.

Typically, capillary suspensions show higher yield stress and low shear viscosity compared to the conventional suspensions. This is a universal phenomenon that can be applied to various material systems. The yield stress for the capillary suspension of pendular bridged particles in wet granular system is expressed as

$$\sigma_y = f(\phi) g(\tilde{V}) \frac{\Gamma cos\theta}{r}$$

where $f(\phi)$ is a function of the volume fraction of particles within the samples and $g(\tilde{V})$ is a function of the normalized droplet volume $\tilde{V} = \frac{V}{r^3}$.[43]

Capillary suspensions can be classified into two types depending on the wetting properties of the substances.[4] They are divided into a pendular state and a capillary state based on the affinity between the secondary fluid and the particle. In the pendular state, the secondary fluid preferentially wets the particles. Whereas, the secondary fluid wets the particles less well than the bulk fluid in the capillary state. The state of the capillary suspensions can be identified by measuring three-phase contact angle θ. The three-

phase contact angle is smaller than 90°in the pendular state and is larger than 90°in the capillary state. The network structure is formed differently in the two states. In the pendular state, individual particles are connected by the secondary fluid bridges and form a network structure. In the capillary state, particles surrounding secondary fluid droplets form clusters and those clusters are connected together to develop a network structure.

The most significant feature of the capillary suspension is a drastic change in flow properties.[6, 10, 44] As described above, a network structure is formed by the secondary fluid in both the pendular and capillary state of the capillary suspension. This particle network structure causes resistance to the flow. Therefore, rheological properties such as the yield stress and viscosity are commonly used for identifying the formation of the capillary suspension. In the suspension with no secondary fluid, Van der Waals attractive force of the particles causes the yield stress. Whereas, in the capillary suspension with certain amount of the secondary fluid, the yield stress is caused by the capillary force. As the amount of secondary fluid increases, both the yield stress and viscosity are increased regardless of the state.

Capillary suspension is well prepared when the secondary fluid is divided into very small droplets by high mixing energy. Particles

are connected or gather around by small droplets of the secondary fluid then form clusters and the sample spanning network structure. When the mixing energy is not enough, capillary network develops only locally and inhomogeneously. In this case, the strength of the capillary suspension becomes weaker than well-prepared capillary suspension.[45]

2.2 **Structure formation of the capillary suspension**

In the previous studies, a computational analysis was performed to investigate the process and principles of the structure formation in the capillary suspension.[3, 46] They calculated the decrease in thermal energy due to the formation of particle clusters as a function of the contact angle between the particles and the secondary fluid, and the relative volume of the secondary fluid compared to the secondary fluid. They found that the largest decrease in energy was obtained when the particles form polytetrahedral structure. They also reported that the contact angle between the secondary fluid and the particles as well as the content of the secondary fluid can also determine the particle network structure.

Chapter 3.

Experimental methods

Chapter 3. Experimental methods

3.1 Materials

Capillary suspensions were prepared using components frequently used in a commercial Li-ion battery anode slurry. Synthetic graphite (SMGPA, China Steel Chemical Corporation, Kaohsiung, Taiwan) with a density of 2.2 g/cm^3, average volume-based diameter d_{50} of 8.92 μm and a specific surface area of 2.24 m^2/g was used as a solid phase. An aqueous carboxymethyl cellulose (CMC, CMC2200, Daicel Corporation, Osaka, Japan) solution was used as a bulk fluid. CMC with a degree of substitution D > 0.8 and an average molecular weight M_w=150,000 g/mol was added to de-ionized water to prepare these solutions. Spherical styrene-butadiene rubber (SBR, TRD2001, JSR Corporation, Tokyo, Japan) with a density of 1.0 g/cm^3, a diameter d_{SBR}=180 nm and 48 wt% solid mass fraction was used as a binder. According to the manufacturer, the SBR binder particles were obtained from emulsion polymerization. A fatty acid surface layer provided stability for the aqueous latex dispersion [25, 47]. 1-octanol (Merck Millipore Corporation, Darmstadt, Germany) with a density of 0.83

g/cm^3 was chosen as the secondary fluid because this fatty alcohol is hardly soluble in water. The concentrations of the graphite particles, CMC and 1-octanol in the slurries were 17.43 vol%, 1.56 vol% and 2 vol%, respectively.

In the experiment for chapter 4.1, the volume fraction of the SBR binder particles was adjusted (0.47 vol%, 0.94 vol%, 1.41 vol%, 1.88 vol% and 2.35 vol%) to assess how this binder affects the flow properties of the capillary-suspension-type graphite slurries and the adhesion of the corresponding dry anode layer to the current collector.

	graphite	CMC	octanol	SBR
Volume percent [vol %]	18.85	1.56	0	0
			2	0.47
				0.94
				1.41
				1.88
				2.35

Table 3.1 Composition of the investigated graphite slurries. The concentration of the ingredients is given in volume fractions (vol%), and water is added such that the total fraction is 100 vol%

In the experiment for chapter 4.2, the total solid volume fraction

was kept constant at 20 vol% in the slurries and the weight ratio of graphite, CMC, and SBR in the dry electrode was 95:2.5:2.5. The concentrations of the SBR in the slurries were 1.01 vol%, The secondary fluid was added to the slurries up to 2 vol%. The composition of the graphite, CMC, and SBR in the dried and slurry state is summarized in Table 3.2.

	graphite	CMC	SBR
electrode mass percent [wt%]	95	2.5	2.5
slurry mass percent [wt%]	32.04	0.84	0.84
slurry volume percent [vol%]	17.43	1.56	1.01

Table 3.2 Composition of the dry electrodes and slurries of graphite/CMC/SBR. The concentration of the ingredients is given in mass (wt%) and volume percent (vol%), and for the slurry, water is added such that the total fraction is 100 vol%.

3.2 Sample preparation

An aqueous CMC solution was prepared by adding 3 wt% of CMC to distilled water. Mixtures were stirred using a propeller type stirrer with a diameter of 50 mm at 1000 revolutions per minute (rpm) for 3 h. The aqueous CMC solution and graphite particles were mixed using a dissolver type stirrer with a diameter of 60 mm

at 1500 rpm for 40 min. This highly concentrated suspension was prepared to assure slurry homogeneity and de-agglomeration of the graphite particles. Subsequently, water was added stepwise in three steps at 10 minute intervals until the concentration of the CMC polymer reached the target value. In this paper, we used the term bulk slurry for this suspension. Battery slurries were prepared by adding the SBR binder to a bulk slurry using a dissolver type mixer (diameter = 40mm) at 650 rpm for 5 min. Capillary suspensions were formed by adding 1-octanol using a dissolver type stirrer (diameter = 40 mm) at 1000 rpm for a certain mixing time t_m.

In the experiment for chapter 4.1, the mixing time was varied between 1 min. < t_m < 10 min. The samples were labeled as shown in Table 3.3.

Sample	composition
bulk	graphite/CMC/water
#SBR (battery)	graphite/CMC/water/# vol% SBR
oct	graphite/CMC/water/octanol(2 vol%)
#SBR/oct	graphite/CMC/water/# vol% SBR/oct
#SBR/oct($)	graphite/CMC/water/# vol% SBR/oct (mixing time $ minute)

Table 3.3 Labelling of the samples with various amounts of SBR binder or mixing times

In the experiment for chapter 4.2, we used the term‘oct+number’ to distinguish the capillary suspensions by placing their volume percent of 1-octanol into a‘number.’For example, we denoted the capillary suspension which contains a 2 vol% of 1-octanol as oct2 and the conventional battery slurry that has no 1-octanol as oct0. The mixing time was 1 min for 1-octanol. To ensure the slurry homogeneity and to remove the mixing dependence, mixing at 1000 rpm for 1 min by a dissolver type stirrer was applied to the conventional slurry in the last step.

3.3 Rheological Characterization

The rheological properties of the slurries were measured using the RheoStress 1 (Thermo Scientific, Germany), Discovery HR-3 (TA instrument, USA) and AR-G2 (TA instrument, USA) stress-controlled type rotational rheometer equipped with parallel plate fixture (35 mm in diameter) and serrated parallel plate fixture (40 mm in diameter) at 20 ℃. To exclude the residual stress due to the sample loading process, all the slurries had a rest time of 120 s before the measurements. Viscosity was measured in the steady

shear rate sweep mode, covering the shear rate range from 0.01 s^{-1} to 1000 s^{-1}. Storage and loss modulus were obtained from the frequency sweep tests at frequency range between 0.1 and 100 rad/s in the linear viscoelastic regime. The linear viscoelastic regime was identified by a strain sweep test at a frequency of 1 rad/s prior to the frequency sweep test. All the measurements were performed at least 3 times.

3.4 Microstructure observation and structure analysis

The slurry microstructure was characterized using a field emission scanning electron microscope (FE-SEM), a Mira3 LMU (Tescan, Brno – Kohoutovice, Czech Republic). The PP3000T (Quorum Technologies, Lewes, UK) was used to freeze the samples. The samples as 10 μl aliquots were loaded into the rivet of the shuttle stub and then frozen in liquid nitrogen after putting the shuttle to the bayonet of the transfer device. Frozen samples were transferred to the cryo-preparation chamber, and cut in the cross-sectional direction using a knife inside the pre-chamber. The samples underwent sublimation at -100 ℃ for 10 min and were then coated with platinum in 10 mA for 120 seconds. All experiments

were conducted at -140 ℃. Afterwards, images taken from FE-SEM were analyzed using the MATLAB (The Mathworks Inc.) software. Particle positions were detected by marking the center of the particles, and all particle distances were measured to calculate the 2D-pair correlation function.

3.5 Emulsion formation and characterization of the interfacial properties

An emulsion consisting of 70 vol% water, 29 vol% octanol and 1 vol% SBR binder was observed using optical microscopy (IX-71, Olympus, Japan). Because the water and 1-octanol are both transparent, alcian blue (Sigma Aldrich, USA) was used to dye the water and discriminate it from 1-octanol. All components were mixed using a homogenizer (Ultraturrax, IKA, Germany) at 6000 rpm for 5 min to form the emulsion.

Interfacial tension was measured to examine the effect of the SBR binder at the interface between the bulk and secondary fluid. The pendant drop method was used to measure the interfacial tension between the water including the SBR binder and 1-octanol [48]. A small glass cuvette was filled with 1-octanol, then a drop of water, which contained SBR binder, was injected into it using a syringe

with a diameter of 1.65 mm. Time evolution of the droplet shape was assessed using a video camera (AVT Stingray F-033B, Allied Vision Technology: 1/2 CCD, 656 492 square pixels) every 10 seconds for 20 minutes. Images were analyzed using commercial software (Drop Shape Analysis, Krüss GmbH, Germany) to calculate the interfacial tension.

The three-phase contact angle refers to the contact angle between the particle and the secondary fluid surrounded by the bulk fluid. This quantity was determined using the sessile drop method. A low-porosity graphite plate (porosity ≤10%, Graphite Cova GmbH, Röthenbach, Germany) was located on the bottom of a transparent cuvette which was filled with the bulk fluid. Then, the secondary fluid was dropped onto the surface of the graphite plate using a syringe. The image of the droplet was taken using a camera (AVT Stingray F-033B), and then, the angle between a drop of the secondary fluid and the graphite plate was analyzed using commercial software (Drop Shape Analysis, Krüss GmbH, Germany).

3.6 Adhesion force measurement

Battery slurries were coated onto a copper foil (10 μm, Itochu Corporation, Japan) used as a current collector for battery anodes and dried to measure the adhesion force between the dried anode

layer and the current collector. Slurries were coated using a ZAA 2300 automatic coater (Zehntner GmbH, Switzerland) and a ZUA 2000 doctor blade (Zehntner GmbH, Switzerland) (width w_B=60 mm, thickness d_B=300 μm) at a coating velocity of 50 mm/s. Coated slurries were dried overnight at room temperature. Dried electrodes were then cut to a width of 25 mm and a length of 60 mm. The adhesion force between the electrode layer and the current collector was measured in a 90°-peel test using a TA.XT plus Texture Analyzer (Stable Micro Systems, UK) universal testing machine. The average force needed to peel the battery electrode from the current collector at a speed of 5 mm/s normalized to the width of the specimen was calculated to characterize the adhesive strength in terms of this line force or line load, respectively. All measurements were performed using a load cell with a maximum force of 5 kg and a force sensitivity of 0.1 g.

3.7 Drying stress

Drying stress was measured with a cantilever deflection method [49, 50] which consists of a cantilever, laser, position sensing detector, and data acquisition system. As a cantilever, 150-μm-thick cover glass was used with a length of 60 mm and a width of 6 mm coated with 20 nm-thick titanium and 100 nm-thick gold by sputtering. For

the calibration, the cantilever was positioned in the drying chamber at a controlled temperature of 25 ± 1 °C and a relative humidity of 20%. A laser (LM-6505MD, Lanics Co.,Ltd.; wavelength = 655 ± 5 nm) was irradiated to the bottom of the cantilever. The degree of cantilever deflection was detected by a position sensing detector (PDP 90A, Thorlabs, Inc.) and translated into an electric signal for data acquisition. Before coating the slurry on the cantilever, the signal of plain cantilever was measured for 30 minutes to assure the reliability of the experiment. After the calibration, the slurry was coated on the cantilever by a doctor blade (ref. 1117/200, Sheen Instruments), and then it was positioned in the drying chamber. As the drying proceeded, the cantilever deflected due to the shrinkage of the slurry, and it shifted the position of the laser beam. The degree of cantilever deflection was detected by the position sensing detector (PDP 90A, Thorlabs, Inc.) and translated into an electric signal for data acquisition. Drying stress was calculated using the Cocoran equation (eq 1):

$$\sigma = \frac{dE_s t_s^3}{3t_c l^2 (t_s+t_c)(1-\nu_s)} + \frac{dE_c(t_s+t_c)}{l^2(1-\nu_c)} \quad (1)$$

, where d, E, t, l, and ν are the deflection, elastic modulus, thickness, substrate length, and Poisson ratio, respectively. Subscripts s and c in the equation represent the substrate and film,

respectively. In this study, the second term in eq 1 was ignored, and only the first term was used to calculate the stress because the modulus of the film (E_c) was much lower than that of the substrate (E_s).

3.8 Porosity measurement

Pore size distribution was measured using a mercury intrusion porosimeter (Autopore IV 9500, Micromeritics Instruments Corporation, USA). When an external pressure was applied to the film and mercury mixture, mercury intruded into the pore of the film. Mercury that had intruded at that pressure was measured to calculate the pore diameter of the film using the Washburn equation (eq 2):

$$P = \frac{-4\gamma\cos\theta}{d} \qquad (2)$$

, where P, γ, θ, and d are the pressure, surface tension of mercury, contact angle of mercury, and diameter of the capillary, respectively. The pore size, size distribution, and porosity can be calculated using the amount of mercury intrusion. The pore size was measured at an external pressure from 0.1 to 33,000 psia (pounds per square inch, absolute). Porosity was calculated using a mercury intrusion volume that represents the void volume. The surface tension of mercury

was 0.485 N/m, and the contact angle was 130 °.

3.9 Three-point bending and repetitive bending test

Conventional slurry and capillary suspensions were coated onto a copper foil (10 μm, Itochu Corporation, Japan) and dried to measure the mechanical strength. Slurries were coated using a ZAA 2300 automatic coater (Zehntner GmbH, Switzerland) and a ZUA 2000 doctor blade (Zehntner GmbH, Switzerland) (width w_B=60 mm; thickness d_B=300 μm) at a coating velocity of 5 mm/s and dried overnight at room temperature. To determine the flexural strength (σ_f) and its strain (γ_f), a three-point-bending test was conducted using a universal testing machine (LF plus, AMETEK, USA). Dried electrodes were cut to a width of 20 mm and a length of 30 mm and bent at a speed of 5 mm/min. The maximum stress for bending the electrode was determined as the flexural strength, and the strain needed to reach the flexural strength was determined as the flexural strain. All measurements were performed using a load cell with a maximum force of 10 N.

A repetitive bending test was performed to characterize resistance against repetitive bending. Electrodes were fixed in a universal testing machine and bent to a certain bending radius

$R_{bending}$ 10 times. After bending, the electrical sheet resistance of the electrodes was measured by applying four-point conductivity measurements.

3.10 FT-IR

Infrared spectroscopy (FT-IR, Nicolet 6700, Thermo Scientific, USA) was conducted to analyze the chemical composition of the capillary suspension during the drying process. The capillary suspension was coated on a KBr pellet of 1 cm x 2 cm and measured every 1 min for 30 min in total. For clear identification of the IR peak, water was replaced with deuterium oxide (D_2O) for this experiment only.

Chapter 4.

Results and discussion

Chapter 4. Results and discussion

4.1 Controlling binder distribution in the capillary suspension

Herein, we investigated the effect of the SBR binder latex added to capillary suspensions that are used as aqueous anode battery slurries. Graphite was suspended in an aqueous CMC solution, together with 1-octanol added as a secondary fluid. The 3-phase contact angle among the graphite particles, 1-octanol and water was measured to be 82°±4°, which suggests that the secondary fluid is located between the particles and forms pendular-shaped bridges. The corresponding strong capillary forces trigger the formation of a sample-spanning network, which we call a capillary network in this paper. This structure formation changes the flow behavior of the suspension dramatically [1]. To understand the effect of the SBR binder on this capillary network, we first investigated the rheological properties of the slurries with and without the SBR latex. Then, we focused on the effect of the SBR binder on the adhesion of the dry film to the current collector for films made from regular and capillary-suspension-type slurries with

and without the SBR binder.

4.1.1 Effect of the SBR binder on the rheological properties

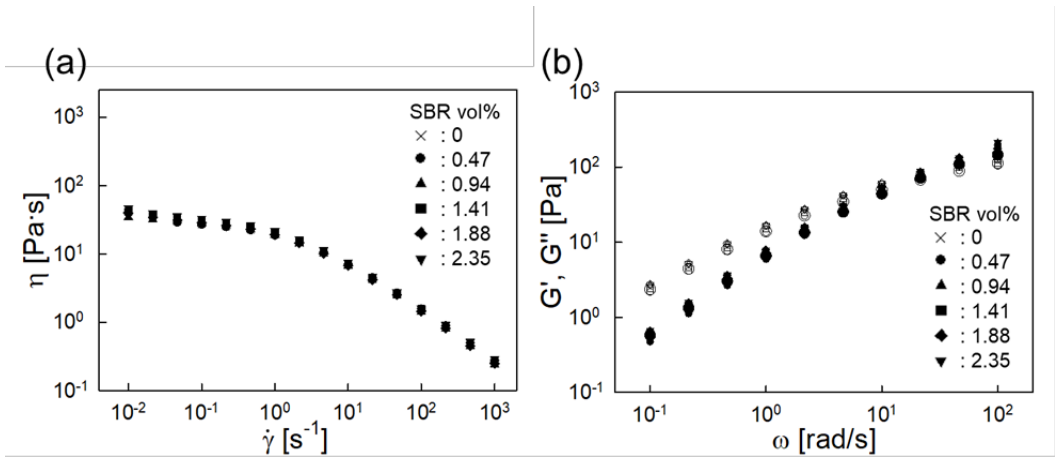

Figure 4.1.1 *(*a*)* Viscosity as a function of the shear rate, *(*b*)* storage *(*closed symbol*)* and loss *(*open symbol*)* modulus at 1% strain as a function of the angular frequency of conventional anode battery slurries for various volume fractions of the SBR binder.

Fig. 4.1.1 shows the effect of the SBR volume fraction on the rheological properties of the bulk and conventional battery slurries. The bulk slurry refers to a suspension with graphite particles suspended in a CMC-water solution, and the battery slurry refers to the bulk slurry with the SBR binder. Viscosity as a function of the shear rate (a) and the storage and loss moduli (b) as a function of

the angular frequency curves all overlap regardless of the volume fraction of the SBR binder. Obviously, the volume fraction of the SBR binder does not affect the rheological properties of the battery slurries in this concentration range of the SBR binder. This result is consistent with findings previously reported by Lim et al. [32]. They found that the SBR binder did not affect the rheological properties of the anode battery slurries unless the CMC concentration, which dominated the flow properties of the battery slurries, was exceptionally low. In contrast, the SBR binder significantly affects the rheological properties of the capillary suspensions shown in Fig. 4.1.2a.

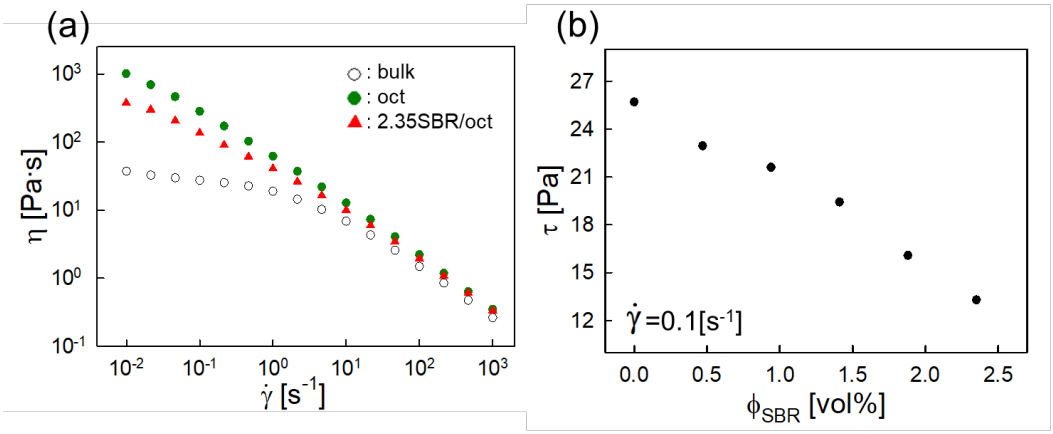

Figure 4.1.1 *(a)* Viscosity curves of a bulk slurry *(*open circle*)* and two capillary suspensions, one with 2 vol% octanol *(*filled circle*)* and the other with 2 vol% octanol and 2.35 vol% SBR binder *(*filled

triangle), and (b) shear stress at a constant shear rate of $\dot{\gamma}$=0.1 s^{-1} for the capillary suspensions including various volume fractions of the SBR binder.

Fig. 4.1.2 shows the effect of the volume fraction of the SBR binder on the rheological properties of the capillary suspensions. Fig. 4.1.2a represents the viscosity change due to the addition of the octanol and SBR binder. The low shear viscosity significantly increased by more than one order of magnitude when the secondary fluid was added to the bulk slurry, whereas the high shear viscosity ($\dot{\gamma}$>100 s^{-1}) remained unchanged. The addition of the SBR binder to the capillary suspension reduced the low shear viscosity while the viscosity at the high shear rates remained constant. This viscosity drop is more pronounced at the higher binder volume fractions shown in Fig. 4.1.2b. The shear stress at a shear rate of 0.1 s^{-1} gradually decreased from 25 Pa to 13 Pa with the increasing volume fraction of the SBR binder from 0 vol% to 2.35 vol%. This confirms that the strength of the capillary suspension is affected by the SBR binder. The mixing conditions for preparing the capillary suspensions can also affect the strength of the capillary suspension as described in Bosslers et al. [45] and shown in Fig. 4.1.3a and b below.

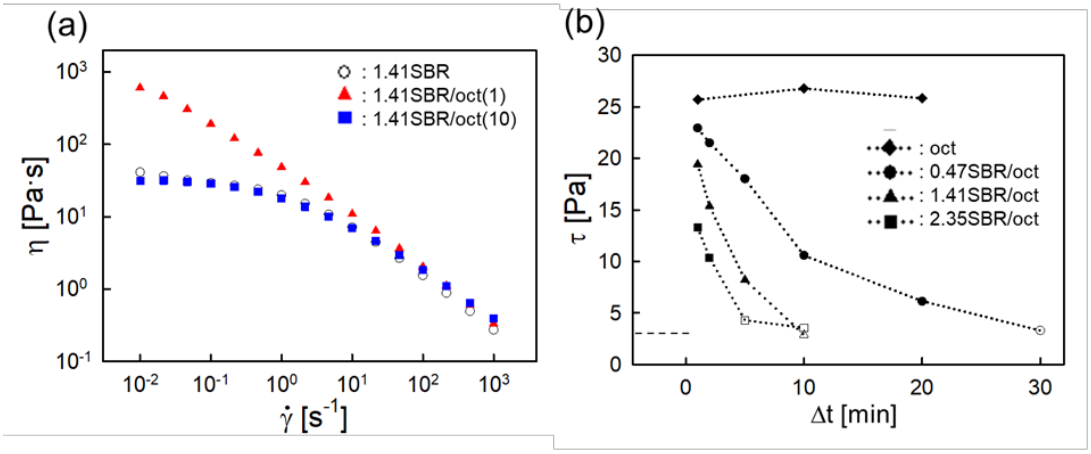

Figure 4.1.2 *(a)* Viscosity curves of the battery slurry and capillary suspensions containing 1.41 vol% SBR binder prepared with different mixing times, Δt=1 min. and Δt=10 min. and *(b)* shear stress at a fixed shear rate of $\dot{\gamma}$=0.1s^{-1} as a function of the mixing time Δt for various capillary suspensions that included different volume fractions of the SBR binder. Suspensions exhibiting the same viscosity curve as the bulk slurry are marked with open symbols.

Fig. 4.1.3 shows the effect of the mixing time on the rheological properties of capillary suspensions containing the SBR binder. The mixing time Δt is defined as the time during which the octanol was added and mixed. As discussed previously, applying a one minute mixing, Δt=1 min., resulted in an increase of the low shear viscosity

by more than one order of magnitude. However, the capillary suspension prepared with Δt=10 min exhibits a viscosity curve essentially coinciding with that of the conventional slurry without octanol (see Fig. 4.1.3a). Fig. 4.1.3b shows the drop of the shear stress measured at a constant low shear rate ($\dot{\gamma}$=0.1 s^{-1}) with an increasing mixing time for the capillary suspensions that included different fractions of SBR. The drop in the shear stress and hence the viscosity is faster at a higher SBR content. In contrast, no effect from the mixing time is observed for the sample without the SBR binder, and the stress is always higher compared to the samples that included the SBR binder. Bossler et al. reported that the yield stress of the capillary suspensions increased when a longer mixing time was applied until it converged to a constant value [45]. Our results are different and demonstrate that the mixing time can be a critical process parameter when additional SBR particles are present. These particles obviously have a strong impact on the formation of the capillary particle network, but apparently, a strong energy input is required to transport the particles to the interface between the two fluids.

Fig. 4.1.4 shows the shear stress at $\dot{\gamma}$ =0.1 s^{-1} with different mixing times and mixing speeds for a slurry that included 1.41 vol% SBR. The stress is plotted vs. the total number of stirrer revolutions after adding the octanol to the slurry. This quantity characterizes the mechanical energy input and apparently determines the observed stress and hence the sample microstructure because the data taken for different stirrer speeds fall onto a mastercurve. After about 25,000 revolutions in total, the viscosity level of the slurry without octanol was reached, and no capillary network was maintained.

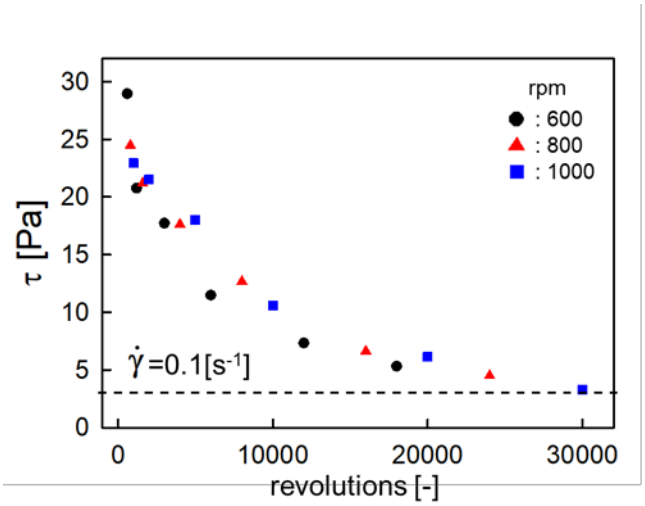

Figure 4.1.3 Shear stress of the capillary suspensions that included 1.41 vol% SBR binder at a shear rate of 0.1 s^{-1} as a function of the revolutions, i.e., the product of the mixing time and speed.

These results confirm that the total energy input determines the flow behavior of the capillary suspensions if they additionally contain the SBR binder, and this property can be adjusted by selecting the appropriate mixing time and speed. Capillary suspensions containing the 1.41 vol% SBR binder prepared with a mixing time of 1 minute at 600 rpm are stable for several weeks and have the same shear stress level even after such a long storage time.

4.1.2 Structure analysis of the capillary suspensions with the SBR added and different mixing times

Microstructural changes of the capillary suspensions due to the different mixing times were observed directly using a cryogenic scanning electron microscope (cryo-SEM). Fig. 4.1.5a-d show cryo-SEM images. Bulk slurry (Fig. 4.1.5a), the capillary suspension without SBR binder (Fig. 4.1.5b) and capillary suspensions with 1.41 vol% SBR binder prepared with different mixing times (c) Δt=1 min (Fig. 4.1.5c) and (d) Δt=10 min (Fig. 4.1.5d) were investigated. Graphite particles, which are shown as white circles, were detected for analyzing the internal structure by

calculating a pair correlation function. Fig. 4.1.5e shows the pair correlation functions g(r) of the bulk slurry and capillary suspensions with and without the SBR. In the case of the oct, 1.41SBR/oct(1) and 1.41SBR/oct(10) samples, the g(r) peaks at the center-to-center distance r=7-8 μm, and then, it approaches one as r is further increased. The peak value of 1.41SBR/oct(1) is similar to oct, while 1.41SBR/oct(10) has a lower maximum g(r) value than 1.41SBR/oct(1) and oct. No apparent peak can be observed for the bulk slurries containing either the SBR binder or the secondary fluid. The peak position of the pair correlation function g(r) resembles the distance between particles in contact, and the absolute value of the g(r) maximum characterizes the number of particles in contact. These data shown in Fig. 4.1.5e confirm the structure formation already indicated by the high low shear viscosity. A longer mixing time reduces the number of particle contacts, thereby weakening the network structure as already seen in the viscosity data (see Fig. 4.1.4). Rheological measurements and structure analysis revealed that the particle network structure in the capillary-suspension-type graphite

slurries is strongly affected by the volume fraction of the added SBR as well as by the energy input used to create the capillary suspensions.

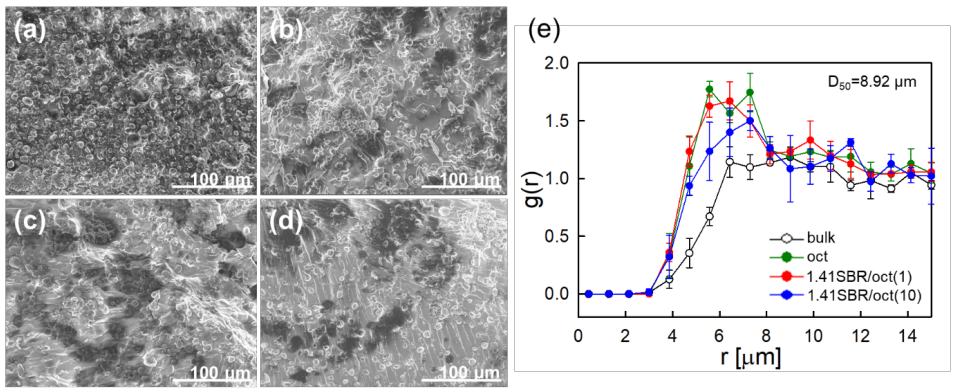

Figure 4.1.5 Cryo-SEM images of the (a) bulk slurry (bulk); (b) the capillary suspension without the SBR binder (oct) and capillary suspension with 1.41 vol% SBR binder prepared with different mixing times (c) Δt=1 min (1.41SBR/oct(1)) and (d) Δt=10 min (1.41SBR/oct(10)). Pair correlation functions [7] were plotted as a function of the center-to-center distance r. D50 denotes the volume-based average diameter of the graphite particles.

4.1.3 Distribution of the SBR particles in the capillary suspension

While a simple mixture of a water and 1-octanol phase separated within minutes Fig. 4.1.6 demonstrates that the 1-octanol droplets dispersed in the water were stabilized when the SBR particles were present in the aqueous phase. A mixture of 70 vol% water, 29 vol% 1-octanol and 1 vol% SBR particles split into an upper phase B densely packed with 1-octanol droplets and a lower phase A with a low concentration of 1-octanol droplets. Nevertheless, these droplets were stable in both phases, and we conclude that the SBR binder particles are located at the interface between the two immiscible liquids thus stabilizing the emulsion and preventing coalescence of the dispersed octanol phase. The SBR binder particles consist of hydrophobic polymers, but they are synthesized to have hydrophilic surface groups. Because of this characteristic, they can be wetted by both hydrophobic and hydrophilic liquids, which enables the formation of a Pickering emulsion of octanol in water. In Pickering emulsions, particles are strongly adsorbed at the liquid-liquid interface rather than desorbed into the water or the oil phase [51]. This suggests that the SBR binder

particles are also located at the interface of the capillary bridges and surrounding bulk phase in the capillary suspensions that include graphite, water, octanol and SBR. The rheological data and structural analysis presented in sections 3.1 and 3.2 further indicate that the deposition of SBR at this interface strongly depends on the energy input used to add the secondary fluid.

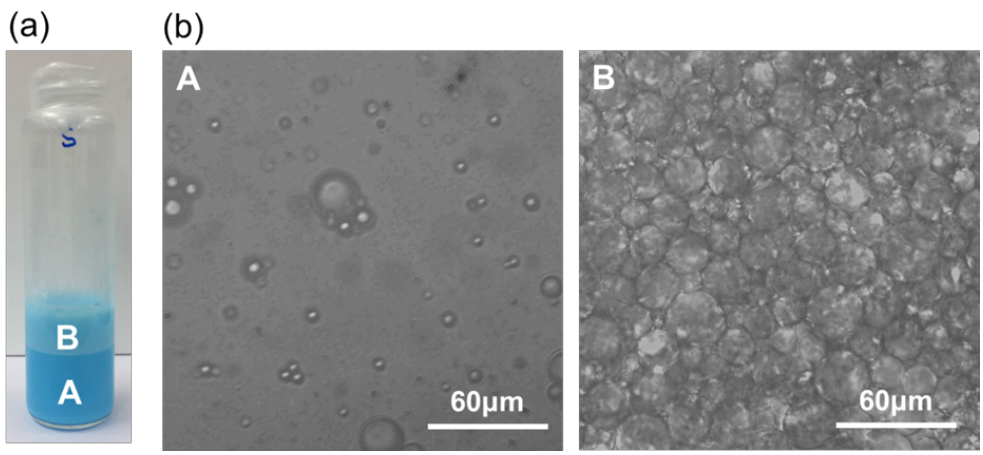

Figure 4.1.4 Mixtures of 70 vol% water, 29 vol% octanol and 1 vol% SBR binder *(a)*. To distinguish the water from the octanol, the water was dyed blue. The sample was mixed at 6000 rpm for 5 min. and left at rest for a day. The photograph on the left shows that the emulsion separated into a lower part *(*A*)* with less droplets and an upper part *(*B*)* with jammed droplets due to creaming. Light microscopy images of phase A and B are shown on the right *(*b*)*.

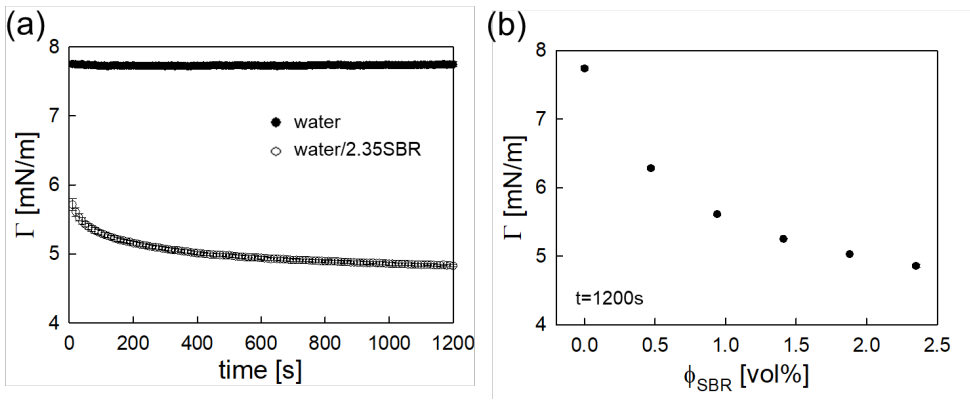

Figure 4.1.5 *(*a*)* Interfacial tension measured by the pendant drop method between water and octanol with and without 2.35 vol% SBR binder as a function of time and *(*b*)* the dependence of the interfacial tension between water and octanol versus the volume fraction of the SBR binder added to the aqueous phase. Interfacial tension was measured after 1200 s when it is considered to have reached an equilibrium state.

Next, we examined how the SBR binder changes the interfacial tension between water and octanol. As shown in Fig. 4.1.7a, the addition of the SBR binder induces a decrease in the interfacial tension with time until a constant value is reached after about 1000 s. The SBR particles are 180 nm-sized colloidal particles which diffuse thermally in the medium. Once the SBR particles are localized at the interface, the emulsifier at the surface of the

particle lowers the interfacial tension. As time goes on, more SBR particles are gathered at the interface, and thereby decreasing the interfacial tension. Fig. 4.1.7b shows the change in the steady-state interfacial tension with the increasing SBR volume fraction. A higher SBR concentration in water resulted in a higher SBR concentration at the interface, which decreased the interfacial tension.

The capillary force, which dominates the strength of the capillary network structure, is a function of the interfacial tension. The changes in the rheological properties in Fig. 4.1.2b and Fig. 4.1.3b can be qualitatively attributed to the changes in the capillary forces related to the localization of the SBR particles at the water/octanol interface and the corresponding drop in the interfacial tension.

Diffusion of the SBR particles in the capillary suspension is around 10^6 times slower than in water because of the high viscosity due to the CMC dissolved in the aqueous phase. It seems that the SBR particles in the capillary suspension hardly reach the interface where they are supposed to be located for minimizing the total energy. Applying an external force, especially mixing in this case, increases the probability of locating the SBR particles at the interface. Therefore, a higher mixing energy results in more SBR particles at the interface, decreasing the interfacial tension, thereby

weakening the network structure and reducing the level of shear stress at low shear rates.

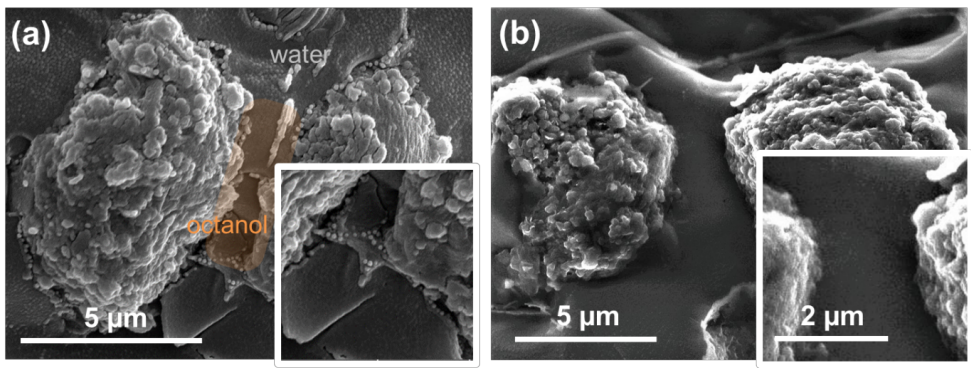

Figure 4.1. 6 Cryo-SEM images of the capillary suspensions containing 1.41 vol% SBR binder with different mixing times *(a)* Δt=1 min. and *(b)* Δt=10 min.

Fig. 4.1.8 shows the microstructure of the capillary suspensions containing 1.41 vol% SBR binder with a mixing time Δt=1 min. and Δt=10 min. The large raspberry-shaped objects are the graphite particles, and the small white spheres are the SBR particles. The distribution of the SBR particles changed completely when different mixing times were applied. They were observed near the graphite surfaces in the case of Δt=1 min, and even a bridge-like SBR structure connecting the graphite particles was observed. Whereas, no SBR particles were found near the graphite particles after Δt=10 min.

As discussed previously, the sample prepared with Δt=1 min. has a stronger network structure than the Δt=10 min. sample. The SBR particles are located in the capillary bridges between the graphite particles when the network structure is strong. Whereas, the sample prepared with Δt=10 min. has a weak structure, and no bridges are left.

There seem to be two reasons for the dramatic drop observed in the low shear viscosity when samples were prepared with a long mixing time: the first reason is the reduction of the interfacial energy Γ (cf. Fig. 4.1.7), and second one is the reduction of the number of capillary bridges as suggested by the cryo-SEM micrographs (cf. Fig. 4.1.5).

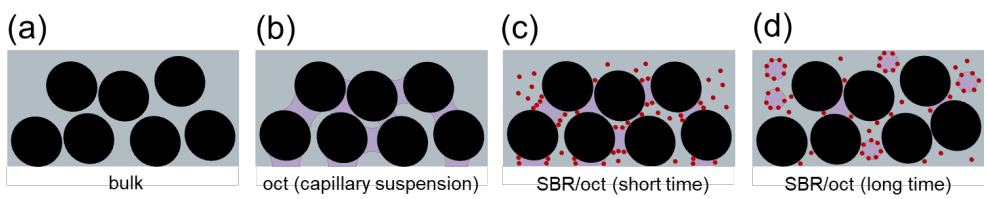

Figure 4.1.7 Schematic of structures for the *(*a*)* bulk slurry *(*bulk*); (*b*)* the capillary suspension without the SBR binder *(*oct*)* and capillary suspension with SBR binder prepared with *(*c*)* short and *(*d*)* long mixing times. Large black circles are graphite particles and small red circles are SBR particles. Octanol is shown in violet

Fig. 4.1.9 suggests the structures of four different slurries

deduced from the results above. When SBR particles are added to the capillary suspension and mixed for a short time, capillary bridges remain and SBR particles are trapped at the interface. Whereas, capillary bridges are destroyed as mixing lasts longer. Mixing accumulates SBR particles at the interface thus reducing the interfacial tensions (see Fig. 4.1.7) and finally capillary forces become insufficient to maintain the network structure.

4.1.4 Adhesion characteristics of the conventional and capillary suspension-type slurries

Fig. 4.1.10 shows the adhesion line force F_a of the electrode layers made from the conventional battery slurries without a secondary fluid as a function of the SBR volume fraction. Obviously, the adhesion force strongly increases with the increasing amount of SBR added to the graphite slurry. No measurable adhesion force was found for samples without added SBR.

Figure 4.1. 8 Adhesion line forces F_a of the battery electrodes

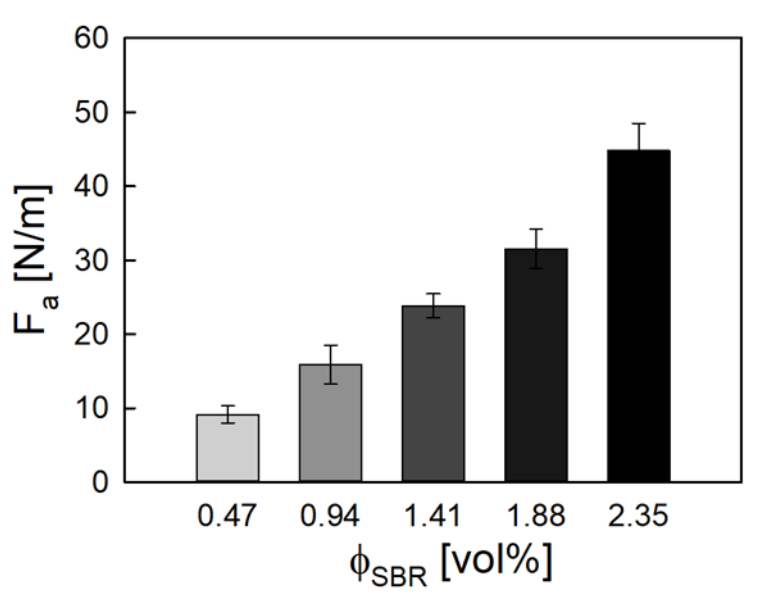

measured using the 90˚-peel test as a function of the SBR volume fractions

The adhesion between the electrode layers and the current collector is decisive for the durability of the battery because it maintains the electrical contact between the graphite layers and copper foil when the electrode expands or shrinks while the Li-ions intercalate or de-intercalate into graphite particles during the charging and discharging processes. Therefore, the adhesion force directly correlates with the cycle life of the battery [52, 53]. It is generally accepted, that the distribution of the SBR binder determines the adhesion strength of the battery electrode. The adhesion strength becomes stronger as the binder concentration at the interface between the electrode and substrate increases [18, 35].

The evidence from the previous sections proves that the distribution of the SBR particles can be very different in the capillary suspensions compared to the regular suspensions. Next, we discuss how this affects the adhesion in the corresponding electrodes made from the capillary-suspension-type graphite slurries.

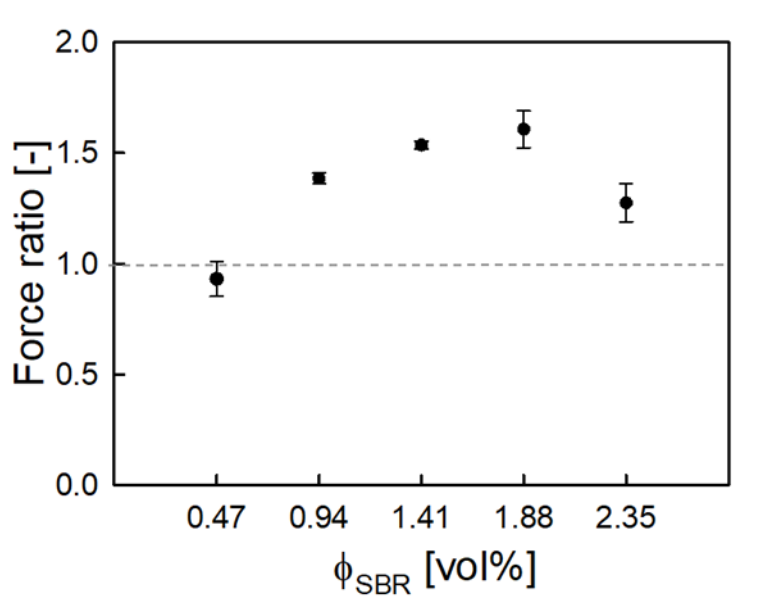

Figure 4.1.9 Dependence of the force ratio defined as the adhesion force from the capillary suspension divided by the adhesion force from battery slurry for various SBR volume fractions

For this comparison, we selected slurries prepared with a mixing time Δt = 1 min. for the added 1-octanol. These slurries were

coated onto copper foils and dried as described above. The adhesion measurements were performed, and the results were related to those obtained using the regular battery slurries with the same amount of SBR. The corresponding force ratio, i.e., the adhesion line force F_a of the capillary-suspension-type slurry divided by the line force F_a obtained for the regular battery slurry, is shown in Fig. 4.1.11 as a function of the SBR volume fraction ϕ_{SBR}. This force ratio increases with an increasing ϕ_{SBR} and reaches a maximum around ϕ_{SBR}=1.5 vol% corresponding to an increase in the adhesion force of about 70% for the electrode made from the capillary-suspension-type slurry compared to the one obtained from the regular battery slurry. The force ratio decreases when the SBR fraction is further increased but is still well above the one for the highest SBR content ϕ_{SBR}=2.35 vol% investigated here.

Figure 4.1. 10 SEM images of the delaminated surfaces for the

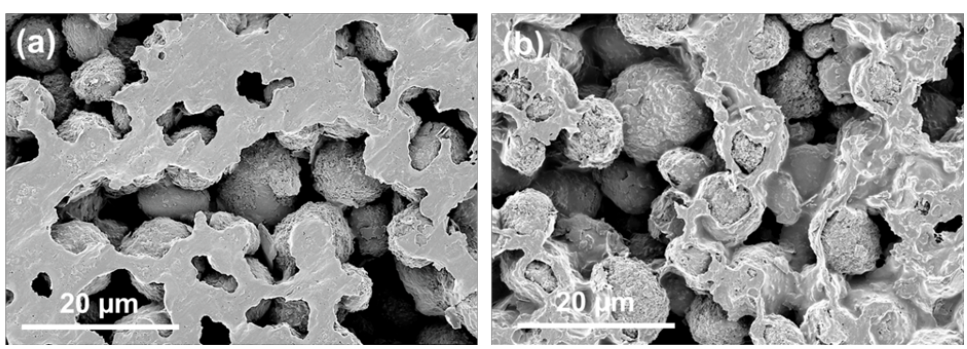

battery electrodes at the copper foil *(*substrate*)*. Battery electrodes were prepared with *(*a*)* battery slurry containing 1.41 vol% SBR

binder and (b) capillary suspension containing 1.41 vol% SBR binder and 2 vol% octanol.

Fig 4.1.11 shows the scanning electron microscopy (SEM) images of the battery electrode surfaces delaminated from the copper foil. Fig. 4.1.12a corresponds to an electrode prepared from a battery slurry without a secondary fluid, whereas the film shown in Fig. 4.1.12b was made from a capillary suspension including 2 vol% 1-octanol as a secondary fluid phase. Fig. 4.1.12a shows the spherical graphite particles and flattened, smooth polymer regions. In contrast, the film made from the capillary suspension (Fig. 4.1.12b) has a less uniform and smooth surface; the polymer regions seem to be ruptured, and several hollow centers are observed.

These SEM images indicate a different failure and delamination characteristic for the electrodes made from the regular and capillary-suspension-type battery slurries. The smooth polymer surface in Fig. 4.1.11a indicates an ideal adhesive failure, whereas the irregular polymer pattern visible in Fig. 4.1.11b may be due to a partial cohesive failure. This indicates a stronger adhesive strength and thus, is consistent with the results shown in Fig. 4.1.10.

One possible reason for this improved adhesion might be a suppression of binder migration often observed during the drying of

the regular battery slurries [34, 35, 37] During solvent evaporation, a capillary pressure induced flow carries the binder particles to the surface of the coating layer causing a binder gradient in perpendicular direction and a depletion of the binder close to the current collector thus limiting the adhesion. Such a migration is suppressed in the capillary-suspension-type slurries because the SBR particles are trapped at the water/octanol interface of the capillary bridges between the graphite particles. The lower vapor pressure of octanol (0.087 mbar at 20 °C) compared to water (23.38 mbar at 20 °C) could further prevent binder migration.

Another reason for the strong adhesion of the capillary-suspension-based electrode layers could be related to the preferential wetting of the octanol (0° contact angle on the copper, ideal wetting) compared to water (50° contact angle on the copper as determined by the sessile drop method). Thus, capillary bridges between the graphite particles and the copper foil may form after the coating, which additionally trap the SBR particles at the interface between the electrode layer and current collector. Further investigations are necessary to verify this hypothesis.

However, the improved adhesion of the capillary-suspension-based electrode layers on the current collector is an experimental fact and may enable an improved battery durability at a lower

binder content. Further investigations including cell cycling tests will be necessary to validate this.

4.1.5 Conclusion

Capillary suspensions are ternary solid/fluid/fluid systems that include two immiscible liquids. Capillary forces in such systems induce the formation of a percolated particle network which results in a paste-like texture and a distinct flow behavior of the suspensions. Recently, this concept has been used to prepare graphite slurries for Li-ion battery anodes with beneficial coating properties [9] and high capacity cells with a superior electrochemical performance [10]. Here, we investigated how additional SBR-particles, widely used as a binder in commercial battery slurries, affect the flow behavior and microstructure of capillary-suspension-type battery slurries that included graphite, an aqueous CMC solution, and 1-octanol as a secondary fluid. Furthermore, we investigated the adhesion of the electrode layers made from such slurries to the current collector.

Our investigations revealed that the particle network, a characteristic for this kind of suspensions, is formed even in the presence of SBR in the aqueous phase. This showed up in a strong, more than one order of magnitude, increase in the low shear

viscosity and was directly confirmed by a pronounced peak in the pair correction function at the particle contact deduced from the cryo-SEM images. However, the SBR slightly weakens the structure, and correspondingly, the low shear viscosity decreases with increasing ϕ_{SBR}, dropping to half the value of the SBR-free slurry when 2.35 vol % SBR is added.

Furthermore, we showed that the energy input during addition of 1-octanol as immiscible, secondary fluid is decisive for structure formation. The strong increase in the low shear viscosity is only achieved at a short mixing time (1 min. mixing time with the equipment used here), but monotonically decreases with increasing energy input, eventually reaching the viscosity level of the slurry without a secondary fluid. Samples with a higher SBR content are more sensitive to the mixing conditions than those with a lower amount of SBR, and the lower viscosity limit is reached faster. Pair correlation functions determined from cryo-SEM images provide direct evidence that there is a reduced number of particle contacts in strongly stirred samples. However, once the slurries are prepared, they are stable for several weeks. Emulsification experiments demonstrated that SBR particles suspended in an aqueous phase can diffuse to the water/octanol interface and stabilize the octanol droplets. The interfacial tension between water

and octanol decreased monotonically from 7.74 mN/m to 4.85 mN/m when ϕ_{SBR} was increased up to 2.35 vol %.

Cryo-SEM images directly show that the SBR particles are located in the contact region between the adjacent graphite particles for the slurries prepared with a low energy input, but not for the slurries made with extended octanol mixing times.

These investigations show that the amount of added SBR and the energy input for mixing the secondary fluid are additional parameters that have to be taken into account when fabricating capillary-suspension-type battery slurries and offer extra degrees of freedom for adjusting the flow properties or microstructure to a desired level.

Finally, we investigated the adhesion of the electrode layers made from capillary-suspension-type graphite slurries to the copper-made current collector as a function of SBR concentration. Generally, the adhesion of the electrodes made from this type of slurry is distinct, i.e., up to 50 %, higher than for electrodes made from corresponding slurries that do not include 1-octanol as a secondary fluid. Whether this is due to the suppressed migration of the binder to the surface of the electrode during drying because SBR is trapped in the capillary bridges between graphite particles or whether additional octanol bridges between the copper foil and

graphite particles promoted by the preferred wetting of octanol on copper, needs further investigation.

Irrespective of that not yet fully disclosed physical origin of the enhanced adhesion, the capillary suspension concept seems to offer a new approach to achieve Li-ion battery electrodes with extended durability at a lower binder content. This may have additional benefits with respect to the electrode conductivity. Further research including cell cycling tests will be performed to get further insight into this technically highly demanded topic.

Li-ion batteries are highly demanded for further expansion of electric vehicles and storage of fluctuating electrical energy supply from renewable resources. Sustainable large scale deployment of these batteries requests formulation of water-based electrode pastes. The flow behavior of such pastes is important to understand with respect to a tailored processing and coating. The adhesion of corresponding dry layers to the collector foil is decisive for battery lifetime and electrochemical performance. Our study focused on the promising capillary suspension concept for paste formulation. Here we demonstrated how SBR, which is a widely used additive for adhesion promotion in conventional battery slurries, affects the flow behavior of capillary suspension type slurries and the adhesion of the corresponding dry layers to the electrode. Microscopic

investigations revealed how the SBR particles modify the water/octanol interface in these slurries. This insight can help to further improve formulation and technical performance of battery electrode slurries but may also stimulate the application of the capillary suspension concept for other slurry based processes and products.

4.2 Drying behavior and mechanical properties of capillary suspension battery electrode

In this paper, we introduce the concept of capillary suspension to a battery anode slurry to control the microstructure, thereby adjusting the drying characteristics to improve the mechanical stability of the electrodes after drying. After dispersing the graphite particles in an aqueous CMC solution with SBR, a secondary fluid, 1-octanol, was added to form a capillary suspension. The three-phase contact angle of graphite, 1-octanol, and water was 82 ± 4°, in which the secondary fluid forms a pendular bridge between the particles. The strong capillary forces generated by the secondary fluid connect the particles and form a sample spanning network inside and then greatly change the flow characteristics of the suspension. To apply capillary suspension processing to the battery slurry and

to understand the microstructure in the liquid state, we first observed the rheological properties of the slurries before and after the addition of the secondary fluid. Afterward, we investigated how the drying characteristics and mechanical properties changed when the capillary suspension concept was applied.

4.2.1 Effect of the secondary fluid on the rheological properties

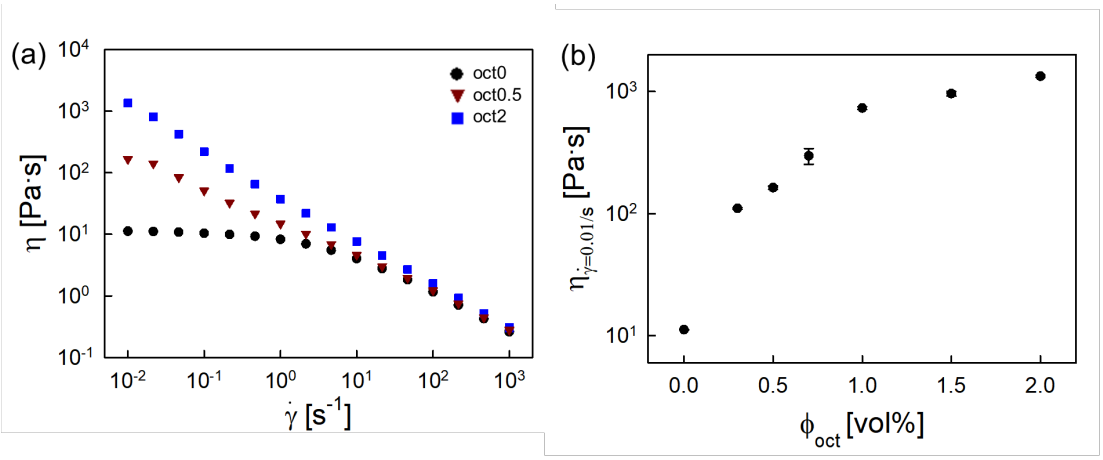

Figure 4.2. 11 *(a)* Viscosity as a function of the shear rate of a conventional slurry *(*oct0*)* and capillary suspensions with 0.5 vol% *(*oct0.5*)* and 2 vol% *(*oct2*)* of the secondary fluid, and *(*b*)* low shear viscosity at a constant shear rate of $\dot{\gamma}$=0.01 s^{-1} for the capillary suspensions at various volume fractions of the secondary fluid.

Fig. 4.2.1a shows the shear viscosity of the conventional slurry

and capillary suspensions. The samples are labeled as "oct + number" according to the content of the secondary fluid, octanol. The number denotes the volume percentage of the secondary fluid. The conventional slurry with no secondary fluid is labeled as oct0, and the capillary suspension with 2 vol% of the secondary fluid is labeled as oct2. When 2 vol% of the secondary fluid was added, the viscosity at a low shear rate of 0.01 s^{-1} increased by about 2 orders of magnitude compared to the conventional slurry, whereas the viscosity at a high shear rate over 100 s^{-1} was similar. The shear stress-shear rate curve (see Figure S1) shows that the flow properties of oct2 completely changed showing a clear yielding behavior in the low shear rate regime. Fig. 4.2.1b indicates the low shear viscosity at a shear rate of 0.01 s^{-1} as a function of the volume percent of the secondary fluid. The low shear viscosity gradually increases and tends to be saturated with the increasing volume fraction of the secondary fluid. When the capillary network structure is formed as the content of the secondary fluid increases, the resistance to the flow becomes stronger, so that the low shear viscosity increases significantly. When the capillary network structure exceeds a certain point, the low shear viscosity reaches a plateau [1, 3]. According to Koos and Willenbacher [42], the plateau regime of the yield stress or low shear viscosity in the capillary

suspension is caused by the transition of the particle network structure into higher order. The increase in low shear viscosity and the following plateau regime in our system can also be attributed to a higher order network structure.

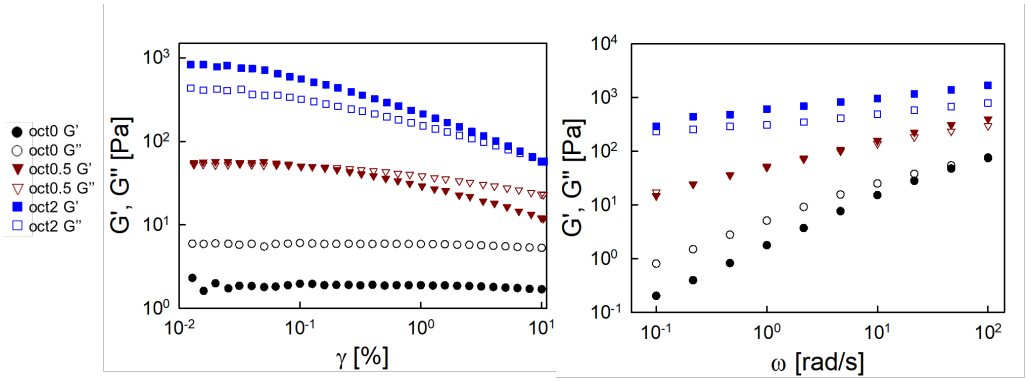

Figure 4.2. 12 Storage *(*closed symbol*)* and loss *(*open symbol*)* moduli of the conventional slurry and capillary suspensions as a function of the *(*a*)* strain and *(*b*)* frequency. Frequency sweep was conducted at γ=0.05%.

Fig. 4.2.2 and Fig. S2 show the effect of the volume fraction of the secondary fluid on the storage and loss moduli of the capillary suspensions. The conventional slurry shows a liquid-like behavior in which G'' is larger than G' in almost the entire strain and frequency range. On the other hand, the capillary suspension containing 2 vol% of the secondary fluid shows a solid-like behavior with a larger value of G' than G'' in the entire strain and frequency range. The

addition of the secondary fluid changes the flow behavior from a liquid-like to a solid-like in the suspension. The flow characteristics of capillary suspensions shown in Fig. 4.2.1 and Fig. 4.2.2, high shear viscosity at a low shear rate and solid-like properties, provide sedimentation stability and good contour accuracy for the battery slurry as described by Bitsch et al [14]. The change in the microstructure can also affect the drying process and mechanical properties after drying as shown in Figs. 4.2.3 and 4.2.4.

4.2.2 Drying stress and porosity of the electrode depending on the amount of the secondary fluid

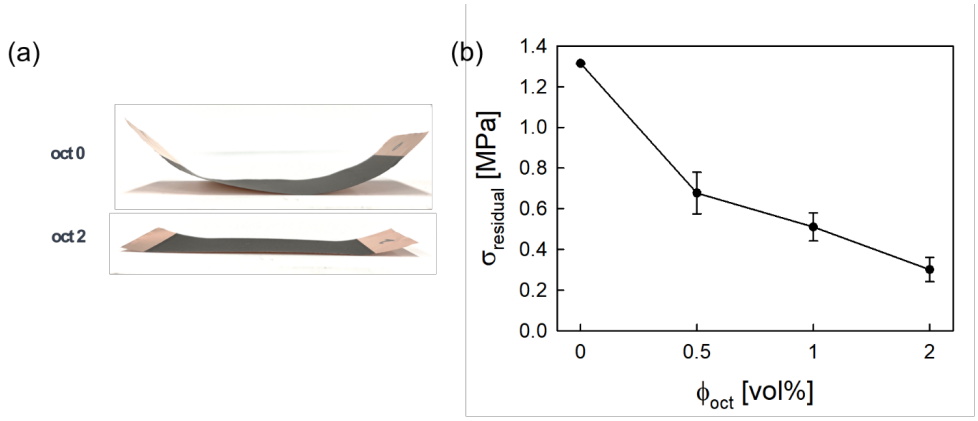

Figure 4.2.13 *(a)* Pictures of the electrodes from the conventional slurry *(*oct0*)* and the capillary suspension containing 2 vol% of the secondary fluid *(*oct2*)* after drying, and *(*b*)* residual stress of the conventional slurry and capillary suspensions with various volume fractions of the secondary fluid after drying.

Fig. 4.2.3a shows images of the electrodes prepared from the conventional slurry and capillary suspension. The conventional electrode is bent into a concave shape while the capillary suspension electrode shows a flat shape. The curvature of the film is caused by the tensile stress that occurs during the drying of the thin film and shows the residual stress generated inside the thin film [54]. Therefore, it can be inferred that the residual stress of the

oct2 electrode is lower than that of the oct0 electrode. To investigate the effect of the microstructure change on the residual stress of the thin film, the stress generated during the drying was quantitatively measured using the cantilever deflection method as shown in Fig. 4.2.3b. The residual stress ($\sigma_{residual}$) indicates that the stress remained after the drying process. The residual stress gradually decreased from 1.3 to 0.3 Pa with the increasing volume fraction of the secondary fluid from 0 to 2 vol%. Since the residual stress is a factor that can cause mechanical instability such as film curls, cracks, peeling off, and buckling of the thin films [55], it is important to manage this efficiently. It confirms that the residual stress of the electrode can be directly controlled by the secondary fluid.

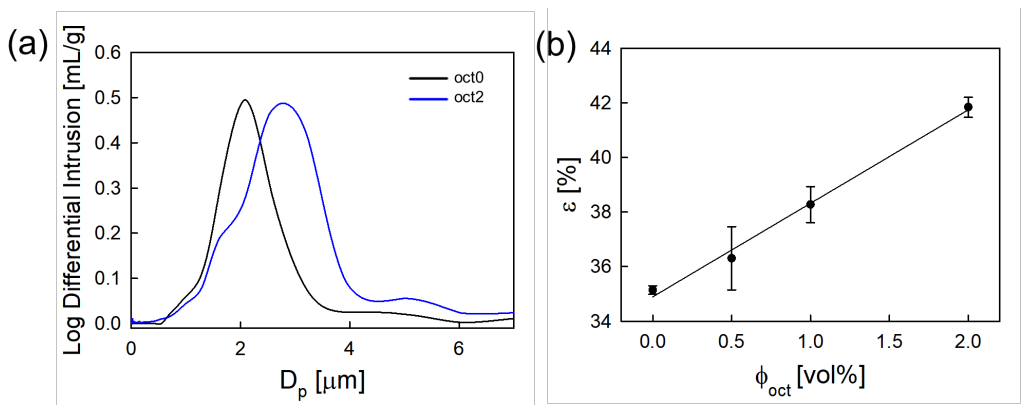

Figure 4.2.14 *(a)* Pore size distributions of the electrodes from the conventional slurry and capillary suspension containing 2 vol% of

the secondary fluid and *(*b*)* porosity *(*ε*)* of the electrodes depending on the volume fraction of the secondary fluid.

	median pore diameter [μm]
oct0	2.11 ± 1.25
oct0.5	2.23 ±1.4
oct1	2.52 ± 1.52
oct2	2.76 ± 1.66

Table 4.1 Median pore diameter of the electrodes as a function of the volume fraction of the secondary fluid.

Fig. 4.2.4 shows the effect of the secondary fluid on the pore size distribution and porosity of the dry electrode prepared from the conventional slurry and capillary suspensions. Fig. 4.2.4a shows the pore size (D_p) distributions of oct0 and oct2. In the case of oct2, the curve is shifted to the right and broadens compared to oct0 indicating that the pore size and porosity are both increased. Table 2 shows the median pore diameter and its standard deviation calculated from the pore size distribution curve. The median pore diameter gradually increases with higher standard deviation

depending on the addition of the secondary fluid from 0 to 2 vol%. In a previous study by Bitsch et al. [15] using a similar material system, the capillary suspension based samples also showed larger median pore size with broad pore size distribution than conventional ones. The addition of the secondary fluid induces the higher order network structure depending on the amount of secondary fluid. It seems that the increase in pore size and broad pore size distribution is a result of the change in the network structure. Fig. 4.2.4b shows the porosity as a function of the volume fraction of the secondary fluid. Porosity increased from 35% to 42% when the secondary fluid increased from 0 to 2 vol%. This result is consistent with findings previously reported. Maurath et al. applied the concept of capillary suspension to manufacture highly porous glass filters[6], and Koos and Willenbacher also used the same method to produce lightweight foam with enhanced porosity [1].

The data shown in Figs. 4.2.3 and 4.2.4 confirm that the residual stress and the internal structure of the electrodes after the drying process are affected by the addition of the secondary fluid in the slurries. We also investigated how the secondary fluid changes the microstructure of the slurries and the drying process in Figs. 4.2.5 and 4.2.6.

4.2.3 Structure analysis of the capillary suspensions in the drying process

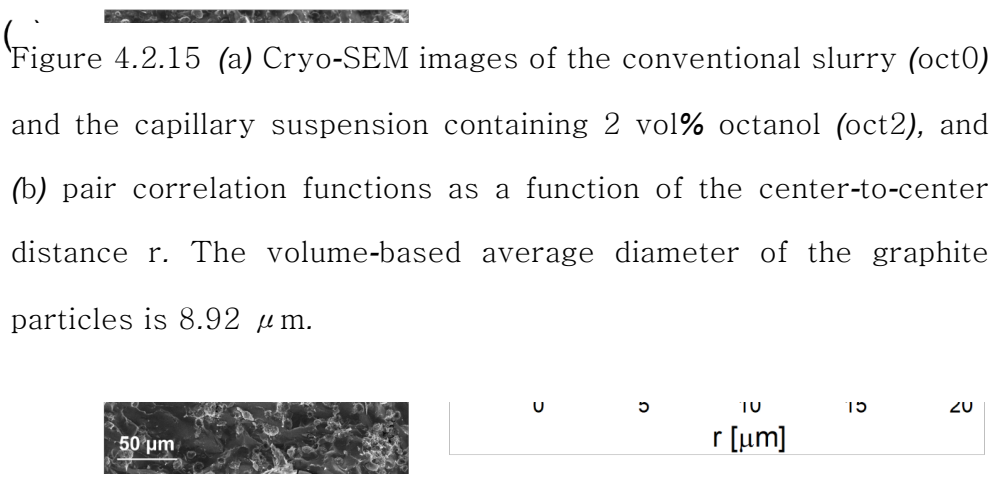

Figure 4.2.15 (a) Cryo-SEM images of the conventional slurry (oct0) and the capillary suspension containing 2 vol% octanol (oct2), and (b) pair correlation functions as a function of the center-to-center distance r. The volume-based average diameter of the graphite particles is 8.92 μm.

The microstructure of the slurry was observed directly by cryogenic scanning electron microscope (cryo-SEM). Fig. 4.2.5a shows the images of oct0 and oct2. The white circles observed in the images are the graphite particles. It seems that the particles are distributed more uniformly in oct0 than in oct2. To analyze the internal structure, the pair correction function was calculated using particle positions detected from the cryo-SEM images. Fig. 4.2.5b shows the pair correlation function g(r) as a function of r. Here, r is the center to center distance between the particles. In the case of oct2, g(r) peaks at r=8 μm and then approaches 1 as r increases. No apparent peak appears in oct0. The position of the peak in the pair

correction function shows the distance between particles in contact, and the value of the g(r) maximum characterizes the number of particles in contact. Fig. 4.2.5b reconfirms the structure change in the capillary suspension already determined by the rheological properties in Figs. 4.2.1 and 4.2.2. The data shown in Fig. 4.2.5 clearly identify that the secondary fluid in the capillary suspension forms a sample-spanning network structure by connecting the particles.

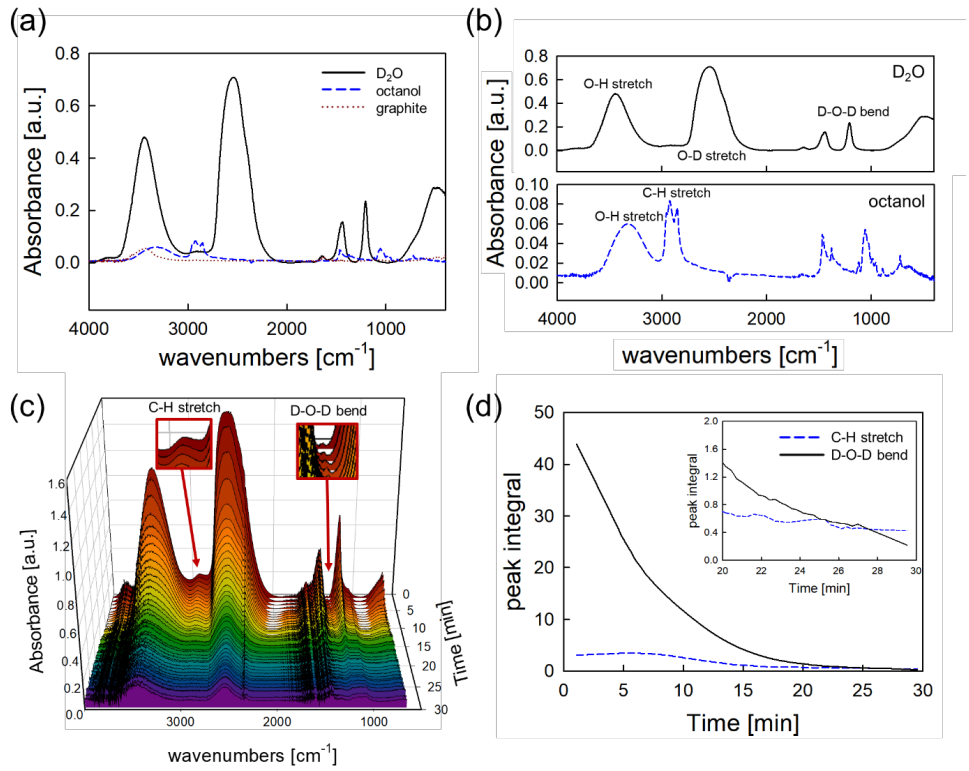

Figure 4.2.16 Infrared absorption spectra of *(*a*)* pure substances of the capillary suspension *(*oct2*)* prepared with deuterium oxide *(*D_2O*)* instead of water and *(*b*)* spectra of the liquids with the peak information. *(*c*)* Infrared absorption spectra of oct2 measured every 1 min for 30 min, and *(*d*)* peak integral of the characteristic octanol *(*C-H stretch*)* and D_2O *(*D-O-D stretch*)* peaks as a function of the drying time.

Next, we examined the composition change of the capillary suspension while drying and analyzed the result before and after drying. Fig. 4.2.6 shows the results of infrared spectroscopy for the capillary suspension containing 2 vol% of octanol. For clear

identification of the IR peak, water was replaced with deuterium oxide (D_2O) in this experiment. Fig. 4.2.6a and 4.2.6b shows the absorbance spectra of pure substances and their functional groups according to the peak position. D_2O has distinguishable peaks of an O-D stretch at 2540 cm^{-1} and a D-O-D bend at 1206 cm^{-1}[156], and 1-octanol has a C-H stretch peak representing the methylene stretching at 2850-3000 cm^{-1}[18]. The absorbance spectra of the capillary suspension (oct2) measured as a function of time are shown in Fig. 4.2.6c. It can be confirmed that the octanol characteristic peak around 2900 cm^{-1} and the D_2O characteristic peak around 1200 cm^{-1} disappeared after 30 min as the drying proceeded. To observe this more clearly, areas under the C-H stretch peak of octanol and the D-O-D bend peak of D_2O were calculated and compared as a function of the drying time in Fig. 4.2.6d. The peak integral of the D-O-D bend decreases sharply in the constant rate period until 8 min and then decreases slowly as the drying progressed, while the peak integral of the C-H stretch maintains the initial value in the early stage of drying and then decreases after 8 min, reaching zero at around the same time as the D-O-D bend. In the later stage of drying, the secondary fluid dried slower than the bulk fluid (see Fig. 4.2.6d inset).

These results are consistent with findings previously reported

by Fischer and Koos. [40]. They conducted drying experiments of capillary suspensions using mass spectrometry (MS) with thermogravimetric analysis (TGA), and found that the secondary fluid evaporated rapidly after the constant rate period. The drying process can be divided into the constant rate period and the falling rate period [57]. In the constant rate period, the coating suspension behaves as if it was full of fluid. The suspension shrinks due to a gradual removal of the solvent in this period. After the constant rate period, the coating suspension stops shrinking, the surface appears dry, and the falling rate period starts. Maintaining the peak integral of the C-H stretch in the constant rate period indicates that the secondary fluid located between the particles tends to maintain the structure during the constant rate period.

In addition, in the previous study by Fischer and Koos [39], it was found that the capillary suspension extends the constant rate period compared to the pure suspension. In the drying process, when the consolidation layer forms at the surface during drying, inner pores of the samples need to be penetrated by air for complete drying. The capillary bridges formed by the secondary fluid require higher air pressure for air invasion. This results in a maintained corner flow, which leads to a longer constant rate period for the capillary suspensions. A prolonged constant rate period in the capillary

suspensions leads to maintaining the network structure longer than pure suspension.

Therefore, the prolonged constant rate period in our capillary suspension results in maintaining the particle network structure longer than the conventional slurry. Also, the secondary fluid hardly evaporates and maintains the network structure in the constant rate period, resulting in a more porous structure in the dried electrode. This change in pore morphology induced by the network structure of the capillary suspension can also affect the mechanical properties of the dried electrode shown in Fig. 4.2.7 below.

4.2.4 Mechanical properties of the conventional and capillary suspension type electrodes

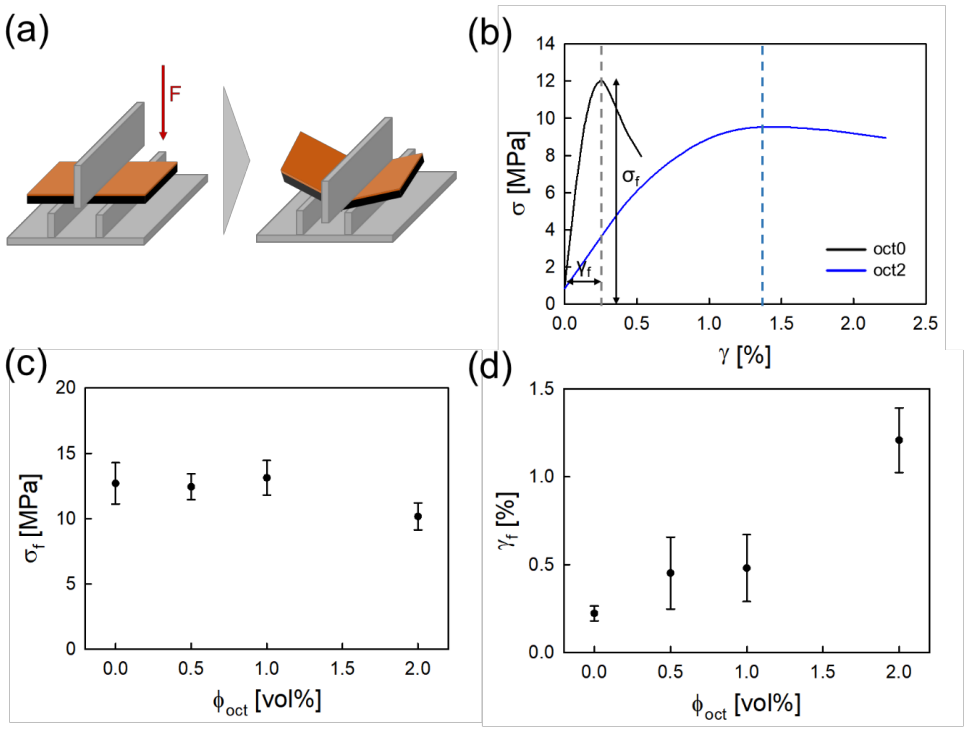

Figure 4.2.17 *(a)* Schematic drawing of a three-point-bending test, and *(b)* flexural stress as a function of the flexural strain for the electrodes from the conventional slurry *(*oct0*)* and capillary suspension *(*oct2*). (c)* Flexural strength *(*σ_f*)* and *(*d*)* strain at σ_f *(*γ_f*)* as a function of the volume fraction of the secondary fluid.

Fig. 4.2.7 shows the effect of the secondary fluid on the mechanical strength such as the bending strength and strain of the

electrodes after drying. Fig. 4.2.7b shows the stress as a function of the strain while bending the electrodes as shown in Fig. 4.2.7a. The maximum stress and strain, the flexural stress σ_f, and the strain γ_f, become completely different in the capillary suspension electrode (oct2 compared to oct0). Fig. 4.2.7c and 4.2.7d shows the changes in σ_f and γ_f depending on the content of the secondary fluid. As the amount of secondary fluid increases, σ_f tends to maintain the constant value and then falls a little at $\phi_{oct} = 2$ vol%, while γ_f gradually increases. In particular, γ_f increases by six times at $\phi_{oct} = 2$ vol% compared to the one obtained from the conventional battery slurry without the secondary fluid.

σ_f is related to the porosity in porous materials [58, 59]. The correlation between the flexural strength and porosity in the Griffith theory, a theory on a material's crack formation and elastic energy release, is as follows [60]:

$$\sigma_f = \sigma_0(1-\varepsilon)^c \qquad (3)$$

, where σ_0 is the theoretical flexural strength at full density; ε is the porosity, and c is a constant. As the content of the secondary fluid increases, the porosity increases (cf. Fig. 4.2.4c), thereby reducing the flexural strength.

The residual stress of the thin film is a result of the

rearrangement and deformation of the internal structure during the drying process that is constrained by a substrate that does not deform [55]. In the drying process, solvent evaporation and the capillary pressure contract the boundaries of the coating film [39], while the substrate does not deform during film shrinkage. This difference induces stress buildup inside the film. One reason for the increase in γ_f in the capillary suspension-based electrodes can be a suppression of particle rearrangement during drying by the secondary fluid that remains between the particles and holds them until the later stage of drying (cf. Fig. 4.2.6). This lowers the residual stress of the electrode (cf. Fig. 4.2.3b), thereby enhancing the tolerance against external stress such as bending.

Another reason could be related to a decrease in the particle packing fraction in the capillary-suspension-based electrode compared to the conventional electrode. Singh et al. [61] reported the relationship between tha particle packing fraction (ϕ_f) and critical crack thickness (CCT). The CCT means the maximum thickness for a film to crack. They showed that the CCT increases with a decrease in ϕ_f. They explained that lower ϕ_f induces a decrease in capillary pressure, which results in a lower stress. Because the decrease in the particle packing fraction is a factor for lowering

stress, a lower particle packing fraction of the capillary suspension can also be considered as a reason for the increase in γ_f.

According to the recent study of Park et al. [62], the SBR binder is selectively localized on the capillary bridges of the secondary fluid in the battery slurry, which enhances the adhesion properties of the electrode after drying. Improvement in adhesion properties can be the other reason for the increase in γ_f.

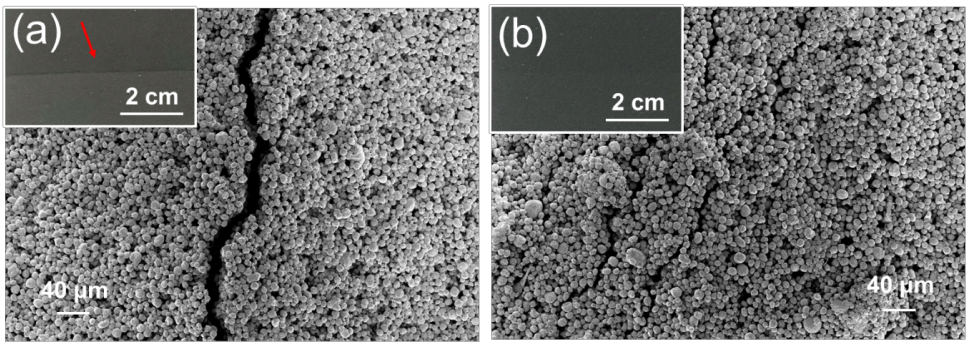

Figure 4.2. 18 Photographs (inset) and SEM images of the electrodes from the (a) conventional slurry (oct0) and (b) capillary suspensions containing 2 vol% of the secondary fluid (oct2) after the three-point bending test.

Fig. 4.2.8 shows the images of the electrode surface prepared with the conventional slurry and capillary suspension after the three-point bending experiments taken from a camera and scanning

electron microscopy (SEM). Fig. 4.2.8a corresponds to an electrode made from the conventional slurry, oct0, whereas the film shown in Fig. 4.2.8b is prepared from the capillary suspension with 2 vol% 1-octanol as the secondary fluid, oct2. Fig. 4.2.8a shows a distinct fracture in the middle of the sample that can also be observed with the naked eye (see the arrow in Fig. 4.2.8a inset) and by SEM. In the case of oct0, cracks are easily generated and propagated even in a small deformation due to the high level of residual stress and stress concentration [63] in which the stress became higher near the flaw. In contrast, the film made from the capillary suspension (Fig. 4.2.8b) has small cracks that can only be identified with high magnification using SEM. Low residual stress and pore morphology change might be the reason for this improved bending flexibility in oct2.

In Fig. 4.2.7b and 4.2.7c, bending stress of oct0 increases sharply with small strain and reaches a maximum at lower flexural strain compared to oct2. Different crack formation observed in Fig. 4.2.8 can be the reason for this phenomenon. Large and deeper cracks in oct0 cause a significant increase in stress with small bending strain and lower flexural strain.

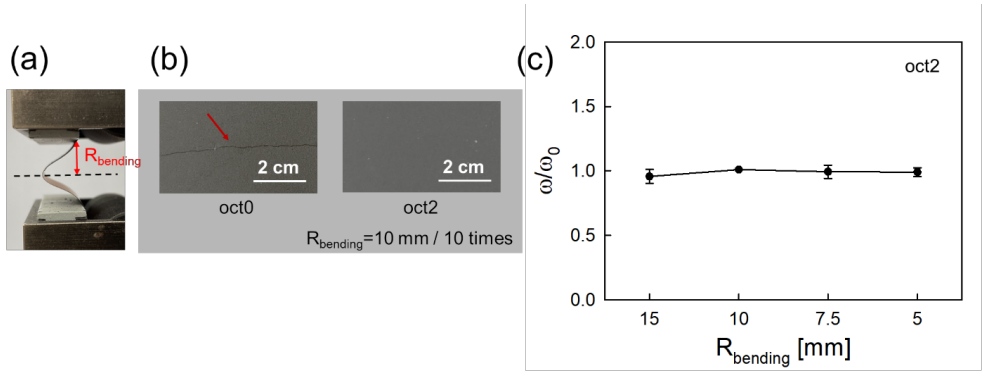

Figure 4.2.19 *(a)* Photograph of the repetitive bending test set-up and, *(b)* conventional *(oct0)* and capillary suspension *(oct2)* based electrodes after bending 10 times with a bending radius of 10 mm. *(c)* Normalized sheet resistance of oct2 depending on the bending radius.

As discussed above, applying the capillary suspension to the electrode results in an increased bending tolerance compared to the conventional electrode. Here, we investigated the effect of the bending on the electrical resistance of the electrode prepared with the capillary suspension using the repetitive bending test set-up [64, 65] as shown in Fig. 4.2.9a. Beginning at a sample length of 40 mm, the samples were bent 10 times to the bending radius ($R_{bending}$) which is defined as one-half of the length after bending. Fig. 4.2.9b shows the surface of the electrodes prepared from the conventional slurry and the capillary suspension that included the 2 vol% of the

secondary fluid after bending 10 times at a bending radius of 10 mm. As in Fig. 4.2.8, oct0 cracked with a clear fracture against the bending, whereas no differences were founded in oct2. The same phenomena happened even if the bending radius gradually decreased to 15, 10, 7.5 and 5, applying a larger deformation.

Fig. 4.2.9c shows the changes in the electrical characteristics on the electrode surface upon the repetitive bending. Because oct0 fractured at every bending radius, the capillary suspension based electrodes, oct2, were measured only. Using a four-point measurement, the ratio of the sheet resistance (ω) relative to the sheet resistance (ω_0) before bending was measured depending on the bending radius. The normalized sheet resistance remains constant even though the bending radius decreases. This indicates that the capillary suspension processing provides resistance to large deformations by controlling the microstructure, thereby enhancing the stability in the electrical performance [66].

In summary, we investigated the effect of the microstructural change in a battery slurry prepared with capillary suspension processing on the drying characteristics and mechanical properties after drying. The secondary fluid, which is located between the particles and forms a network structure in the capillary suspension, remains until the later stage of drying and maintains the network

structure, thus suppressing the rearrangement of particles during drying. This results in a lower residual stress and morphology change in the pore structure of the dry electrode and therefore greatly increases the resistance to deformations such as bending. These investigations demonstrate that the mechanical stability and flexibility of the electrode can be improved by adding a small amount of secondary fluid using the capillary suspension processing.

4.2.5 Conclusion

A capillary suspension is a ternary system that consists of particles and two immiscible liquids. A small amount of secondary fluid added to a suspension causes a capillary force between the particles to form a percolated particle network, through which the flow behavior of the suspension is changed to a paste-like texture. In this paper, we applied the concept of capillary suspension to graphite-based battery slurries to investigate how the drying and mechanical properties change when manufacturing electrodes.

When 1-octanol is added as a secondary fluid to a conventional battery slurry, the low shear viscosity and modulus increase as the particle network structure forms to create a capillary suspension. As the content of the secondary fluid increases, this phenomenon becomes more pronounced so that the low shear viscosity increases

about 2 orders of magnitude at ϕ_{oct} =2 vol%. Particles that are attached to each other and forms a network structure in the capillary suspension were directly observed by cryo-SEM images.

The particle network structure in the capillary suspension tends to be maintained even after drying. FT-IR results confirmed that the secondary fluid sustained the network structure until the bulk fluid completely dried. This inhibits the rearrangement of particles during the drying process and significantly lowers the drying stress in the capillary suspension-based electrode. Additionally, the pore size and porosity also increase due to the network structure even after drying.

The structural change observed above also has a great influence on the mechanical properties of the electrode. Electrodes to which the capillary suspension is applied have an enhanced mechanical stability. When the electrodes were deformed by the three-point bending set-up, the yield strain of the capillary suspension-based electrode significantly increased compared to the conventional electrode. In addition, only small surface cracks were observed under a microscope for the capillary suspension electrode in contrast to the conventional one in which a clear fracture occurred above the yield strain. This is due to the decrease in residual stress and the changes in the internal structure. The sheet resistance of

the capillary suspension electrode before and after the bending shows a constant value, which indicates that the electronic path by the particles is not destroyed even at a large bending deformation.

This paper presents a new method for fabricating a Li-ion battery electrode with enhanced mechanical stability. Mechanical stability, the degree of defect and the quality of the electrode can be directly related to the performance of the battery. We applied the concept of capillary suspension to battery slurry and improved these properties. This might provide several advantages on cell cycling of the battery.

Although we used a model system without conductive agent such as carbon black, this work can provide the insight to microstructure design or flow control of battery slurry even with a battery slurry including conductive agent. Further research will include electrical performance of this electrode to get further insight into this topic. This can also be applied to emerging electrode systems for next-generation battery technology such as a thick electrode or flexible electrode. Since these technologies demand higher standard of mechanical stability against harsh conditions such as repetitive bending or folding, the capillary suspensions can be a great alternative for battery slurries. In addition, the insight in this paper may help us to formulate other slurries, in which the importance of

mechanical stability is emphasized.

Chapter 5.

Summary

Summary

In this thesis, application of capillary suspensions to Li-ion battery electrode was introduced. The microstructure of slurries as well as the mechanical properties of the electrode were controlled using the concept of capillary suspension. In the slurry state, SBR binder distribution can be controlled using capillary network. In addition, mechanical properties of the electrodes such as adhesion and bending properties are controlled by capillary network even after drying process.

Firstly, our investigations revealed that the particle network, a characteristic for this kind of suspensions, is formed even in the presence of SBR in the aqueous phase. However, the SBR slightly weakens the structure, and correspondingly, the low shear viscosity decreases with increasing the amount of SBR, dropping to half the value of the SBR-free slurry when 2.35 vol % SBR is added.

Samples with a higher SBR content are more sensitive to the mixing conditions than those with a lower amount of SBR, and the lower viscosity limit is reached faster. Emulsification experiments demonstrated that SBR particles suspended in an aqueous phase can diffuse to the water/octanol interface and stabilize the octanol

droplets. The interfacial tension between water and octanol decreased monotonically when the amount of SBR binder was increased. Cryo-SEM images directly showed that the SBR particles are located in the contact region between the adjacent graphite particles for the slurries prepared with a low energy input, but not for the slurries made with extended octanol mixing times.

These investigations show that the amount of added SBR and the energy input for mixing the secondary fluid are additional parameters that have to be taken into account when fabricating capillary-suspension-type battery slurries and offer extra degrees of freedom for adjusting the flow properties or microstructure to a desired level.

The adhesion of the electrode layers made from capillary-suspension-type graphite slurries to the copper-made current collector was investigated as a function of SBR concentration. Generally, the adhesion of the electrodes made from this type of slurry is distinct, i.e., up to 50 %, higher than for electrodes made from corresponding slurries that do not include 1-octanol as a secondary fluid. This is due to the suppressed migration of the binder to the surface of the electrode during drying because SBR is trapped in the capillary bridges between graphite particles or additional octanol bridges between the copper foil and graphite

particles promoted by the preferred wetting of octanol on copper.

Next, we investigated how the drying and mechanical properties change when manufacturing capillary suspension electrodes. The particle network structure in the capillary suspension tended to be maintained even after drying. FT-IR results confirmed that the secondary fluid maintained the network structure until the bulk fluid completely dried. This inhibits the rearrangement of particles during the drying process and significantly lowers the drying stress in the capillary suspension-based electrode. Additionally, the pore size and porosity also increase due to the network structure even after drying.

The structural change observed above also has a great influence on the mechanical properties of the electrode. Electrodes to which the capillary suspension is applied have an enhanced mechanical stability. When the electrodes were deformed by the three-point bending set-up, the yield strain of the capillary suspension-based electrode significantly increased compared to the conventional electrode. In addition, only small surface cracks were observed under a microscope for the capillary suspension electrode in contrast to the conventional one in which a clear fracture occurred above the yield strain. This is due to the decrease in residual stress and the changes in the internal structure. The sheet

resistance of the capillary suspension electrode before and after the bending shows a constant value, which indicates that the electronic path by the particles is not destroyed even at a large bending deformation.

Li-ion batteries are highly demanded for further expansion of electric vehicles and storage of fluctuating electrical energy supply from renewable resources. Sustainable large scale deployment of these batteries requests formulation of water-based electrode pastes. The flow behavior of such pastes is important to understand with respect to a tailored processing and coating. Our study focused on the promising capillary suspension concept for paste formulation.

Here we demonstrated how the microstructure and binder distribution are controlled using capillary suspension and how the secondary fluid affect drying process and mechanical properties even after drying. We showed that the adhesion properties and mechanical stability which are related to battery performance are enhanced by the concept of capillary suspension. This insight can help to further improve formulation and technical performance of battery electrode slurries but may also stimulate the application of the capillary suspension concept for other slurry based processes and products.

References

1. Koos, E.; Willenbacher, N., Capillary forces in suspension rheology. Science 2011, 331, (6019), 897-900.

2. Velankar, S. S., A non-equilibrium state diagram for liquid/fluid/particle mixtures. Soft Matter 2015, 11, (43), 8393-403.

3. Koos, E., Capillary suspensions: Particle networks formed through the capillary force. Current Opinion in Colloid and Interface Science 2014, 19, (6), 575-584.

4. Bossler, F.; Koos, E., Structure of Particle Networks in Capillary Suspensions with Wetting and Nonwetting Fluids. Langmuir 2016, 32, (6), 1489-501.

5. Dittmann, J.; Maurath, J.; Bitsch, B.; Willenbacher, N., Highly Porous Materials with Unique Mechanical Properties from Smart Capillary Suspensions. Advanced Materials 2016, 28, (8), 1689-96.

6. Maurath, J.; Dittmann, J.; Schultz, N.; Willenbacher, N., Fabrication of highly porous glass filters using capillary suspension processing. Separation and Purification Technology 2015, 149, 470-478.

7. Jampolski, L.; Sänger, A.; Jakobs, T.; Guthausen, G.; Kolb, T.; Willenbacher, N., Improving the processability of coke water slurries for entrained flow gasification. Fuel 2016, 185, 102-111.

8. Schneider, M.; Maurath, J.; Fischer, S. B.; Weiss, M.; Willenbacher, N.; Koos, E., Suppressing Crack Formation in Particulate Systems by Utilizing Capillary Forces. ACS Applied Materials & Interfaces 2017, 9, (12), 11095-11105.

9. Schneider, M.; Koos, E.; Willenbacher, N., Highly conductive, printable pastes from capillary suspensions. Scientific Reports 2016, 6, 31367.

10. Hoffmann, S.; Koos, E.; Willenbacher, N., Using capillary bridges to tune stability and flow behavior of food suspensions. Food Hydrocolloids 2014, 40, 44-52.

11. Domenech, T.; Velankar, S., Capillary-driven percolating networks in ternary blends of immiscible polymers and silica particles. Rheologica Acta 2014, 53, (8), 593-605.

12. Hartung, K.; Benner, C.; Willenbacher, N.; Koos, E., Lightweight Porous Glass Composite Materials Based on Capillary Suspensions. Materials (Basel) 2019, 12, (4).

13. Weiß, M.; Maurath, J.; Willenbacher, N.; Koos, E., Shrinkage and dimensional accuracy of porous ceramics derived from capillary suspensions. Journal of the European Ceramic Society 2019, 39, (5), 1887-1892.

14. Bitsch, B.; Dittmann, J.; Schmitt, M.; Scharfer, P.; Schabel, W.; Willenbacher, N., A novel slurry concept for the fabrication of lithium-ion battery electrodes with beneficial properties. Journal of Power Sources 2014, 265, 81-90.

15. Bitsch, B.; Gallasch, T.; Schroeder, M.; Börner, M.; Winter, M.; Willenbacher, N., Capillary suspensions as beneficial formulation concept for high energy density Li-ion battery electrodes. Journal of Power Sources 2016, 328, 114-123.

16. Son, J.-T.; Cairns, E., Structure and electrochemical characterization of LiNi0.3Co0.3Mn0.3Fe0.1O2 cathode for lithium secondary battery. Korean Journal of Chemical Engineering 2007, 24, (5), 888-891.

17. Chou, S. L.; Pan, Y.; Wang, J. Z.; Liu, H. K.; Dou, S. X., Small things make a big difference: binder effects on the performance of Li and Na batteries. Physical Chemistry Chemical Physics 2014, 16, (38), 20347-59.

18. Haselrieder, W.; Westphal, B.; Bockholt, H.; Diener, A.; Höft, S.; Kwade, A., Measuring the coating adhesion strength of electrodes for lithium-ion batteries. International Journal of Adhesion and Adhesives 2015, 60, 1-8.

19. Lee, J.; Sung, S.; Kim, Y.; Park, J. D.; Ahn, K. H., A new paradigm of materials processing—heterogeneity control. Current Opinion in Chemical Engineering 2017, 16, 16-22.

20. Hanisch, C.; Loellhoeffel, T.; Diekmann, J.; Markley, K. J.; Haselrieder, W.; Kwade, A., Recycling of lithium-ion batteries: a novel method to separate coating and foil of electrodes. Journal of Cleaner Production 2015, 108, 301-311.

21. Son, B.; Ryou, M. H.; Choi, J.; Lee, T.; Yu, H. K.; Kim, J. H.; Lee, Y. M., Measurement and analysis of adhesion property of lithium-ion battery electrodes with SAICAS. ACS Applied Materials & Interfaces 2014, 6, (1), 526-31.

22. Lee, J.-T.; Chu, Y.-J.; Peng, X.-W.; Wang, F.-M.; Yang, C.-R.; Li, C.-C., A novel and efficient water-based composite binder for LiCoO2 cathodes in lithium-ion batteries. Journal of Power Sources 2007, 173, (2), 985-989.

23. Sung, S. H.; Kim, D. H.; Kim, S.; Jeong, M. H.; Nam, J.; Ahn, K. H., Effect of neutralization of poly(acrylic acid) binder on the dispersion heterogeneity of Li-ion battery electrodes. Journal of Materials Science 2019, 54, (20), 13208-13220.

24. Lee, G.-W.; Ryu, J. H.; Han, W.; Ahn, K. H.; Oh, S. M., Effect of slurry preparation process on electrochemical performances of LiCoO2 composite electrode. Journal of Power Sources 2010, 195, (18), 6049-6054.

25. Lee, J.-H.; Lee, S.; Paik, U.; Choi, Y.-M., Aqueous processing of natural graphite particulates for lithium-ion battery anodes and their electrochemical performance. Journal of Power Sources 2005, 147, (1-2), 249-255.

26. Hawley, W. B.; Li, J., Electrode manufacturing for lithium-ion batteries—Analysis of current and next generation processing. Journal of Energy Storage 2019, 25.

27. Zolin, L.; Chandesris, M.; Porcher, W.; Lestriez, B., An Innovative Process for Ultra-Thick Electrodes Elaboration: Toward Low-Cost and High-Energy Batteries. Energy Technology 2019, 7, (5).

28. Adachi, N.; Hashiba, M.; Sakurada, O., Rheological properties of slurries prepared using a planetary mixer. Ceramics International 2004, 30, (6), 1055-1058.

29. Li, L.; Erb, R. M.; Wang, J.; Wang, J.; Chiang, Y.-M., Fabrication of Low-Tortuosity Ultrahigh-Area-Capacity Battery

Electrodes through Magnetic Alignment of Emulsion-Based Slurries. Advanced Energy Materials 2019, 9, (2).

30. Kim, D.; Koo, S., Rheological estimation of aggregate size for a colloidal suspension of carbon black particles. Korea-Australia Rheology Journal 2020, 32, (4), 301-308.

31. Tran, Q. N.; Kim, I. T.; Hur, J.; Kim, J. H.; Choi, H. W.; Park, S. J., Composite of nanocrystalline cellulose with tin dioxide as Lightweight Substrates for high-performance Lithium-ion battery. Korean Journal of Chemical Engineering 2020, 37, (5), 898-904.

32. Lim, S.; Kim, S.; Ahn, K. H.; Lee, S. J., The effect of binders on the rheological properties and the microstructure formation of lithium-ion battery anode slurries. Journal of Power Sources 2015, 299, 221-230.

33. Shim, J.; Striebel, K. A., Effect of electrode density on cycle performance and irreversible capacity loss for natural graphite anode in lithium-ion batteries. Journal of Power Sources 2003, 119-121, 934-937.

34. Lim, S.; Ahn, K. H.; Yamamura, M., Latex migration in battery slurries during drying. Langmuir 2013, 29, (26), 8233-44.

35. Jaiser, S.; Müller, M.; Baunach, M.; Bauer, W.; Scharfer, P.; Schabel, W., Investigation of film solidification and binder migration during drying of Li-Ion battery anodes. Journal of Power Sources 2016, 318, 210-219.

36. Jaiser, S.; Funk, L.; Baunach, M.; Scharfer, P.; Schabel, W., Experimental investigation into battery electrode surfaces: The distribution of liquid at the surface and the emptying of pores during drying. Journal of Colloid and Interface Science 2017, 494, 22-31.

37. Lim, S.; Kim, S.; Ahn, K. H.; Lee, S. J., Stress Development of Li-Ion Battery Anode Slurries during the Drying Process. Industrial & Engineering Chemistry Research 2015, 54, (23), 6146-6155.

38. Bauer, C.; Cima, M.; Dellert, A.; Roosen, A., Stress Development During Drying of Aqueous Zirconia Based Tape Casting Slurries Measured by Transparent Substrate Deflection Method. Journal of the American Ceramic Society 2009, 92, (6), 1178-1185.

39. Fischer, S. B.; Koos, E., Using an added liquid to suppress drying defects in hard particle coatings. Journal of Colloid and Interface Science 2021, 582, (Pt B), 1231-1242.

40. Fischer, S. B.; Koos, E., Influence of drying conditions on the stress and weight development of capillary suspensions. Journal of the American Ceramic Society 2020, 104, (3), 1255-1270.

41. Koos, E.; Kannowade, W.; Willenbacher, N., Restructuring and aging in a capillary suspension. Rheologica Acta 2014, 53, (12), 947-957.

42. Koos, E.; Willenbacher, N., Particle configurations and gelation in capillary suspensions. Soft Matter 2012, 8, (14).

43. Bossler, F.; Maurath, J.; Dyhr, K.; Willenbacher, N.; Koos, E., Fractal approaches to characterize the structure of capillary suspensions using rheology and confocal microscopy. Journal of Rheology 2018, 62, (1), 183-196.

44. Domenech, T.; Velankar, S. S., On the rheology of pendular gels and morphological developments in paste-like ternary systems based on capillary attraction. Soft Matter 2015, 11, (8), 1500-16.

45. Bossler, F.; Weyrauch, L.; Schmidt, R.; Koos, E., Influence of mixing conditions on the rheological properties and structure of capillary suspensions. Colloids and Surfaces A: Physicochemical and Engineering Aspects 2017, 518, 85-97.

46. Bindgen, S.; Bossler, F.; Allard, J.; Koos, E., Connecting particle clustering and rheology in attractive particle networks. Soft Matter 2020, 16, (36), 8380-8393.

47. Kim, J. S.; Hong, S.; Park, D. W.; Shim, S. E., Water-borne graphene-derived conductive SBR prepared by latex heterocoagulation. Macromolecular Research 2010, 18, (6), 558-565.

48. Berry, J. D.; Neeson, M. J.; Dagastine, R. R.; Chan, D. Y.; Tabor, R. F., Measurement of surface and interfacial tension using pendant drop tensiometry. Journal of Colloid and Interface Science 2015, 454, 226-37.

49. Kim, S.; Sung, J. H.; Ahn, K. H.; Lee, S. J., Drying of the silica/PVA suspension: effect of suspension microstructure.

Langmuir 2009, 25, (11), 6155-61.

50. Kim, S.; Sung, J. H.; Hur, K.; Ahn, K. H.; Lee, S. J., The effect of adsorption kinetics on film formation of silica/PVA suspension. Journal of Colloid and Interface Science 2010, 344, (2), 308-14.

51. Chevalier, Y.; Bolzinger, M.-A., Emulsions stabilized with solid nanoparticles: Pickering emulsions. Colloids and Surfaces A: Physicochemical and Engineering Aspects 2013, 439, 23-34.

52. Chen, L.; Xie, X.; Xie, J.; Wang, K.; Yang, J., Binder effect on cycling performance of silicon/carbon composite anodes for lithium ion batteries. Journal of Applied Electrochemistry 2006, 36, (10), 1099-1104.

53. Kim, J.-B.; Jun, B.-S.; Lee, S.-M., Improvement of capacity and cyclability of Fe/Si multilayer thin film anodes for lithium rechargeable batteries. Electrochimica Acta 2005, 50, (16-17), 3390-3394.

54. Injeti, S. S.; Annabattula, R. K., Extending Stoney's equation to thin, elastically anisotropic substrates and bilayer films. Thin Solid Films 2016, 598, 252-259.

55. Abadias, G.; Chason, E.; Keckes, J.; Sebastiani, M.; Thompson, G. B.; Barthel, E.; Doll, G. L.; Murray, C. E.; Stoessel, C. H.; Martinu, L., Review Article: Stress in thin films and coatings: Current status, challenges, and prospects. Journal of Vacuum Science & Technology A: Vacuum, Surfaces, and Films 2018, 36, (2).

56. Park, K.; Kim, Y.; Lee, K. J., Analysis of deuterated water contents using FTIR bending motion. Journal of Radioanalytical and Nuclear Chemistry 2019, 322, (2), 487-493.

57. Schere, G. W., Theory of Drying. Journal of the American Ceramic Society 1990, 73, (1), 3-14.

58. WAGH, A. S.; SINGH, J. P.; POEPPEL, R. B., Dependence of ceramic fracture properties on porosity. Journal of Materials Science 1993, 28, 3589-3593.

59. Hardin, R. A.; Beckermann, C., Effect of Porosity on the Stiffness of Cast Steel. Metallurgical and Materials Transactions A 2007, 38, (12), 2992-3006.

60. KWAN, Y. B. P.; STEPHENSON, D. J.; ALCOCK, J. R., The porosity dependence of flexural modulus and strength for capsule-free hot isostatically pressed porous alumina. Journal of Materials Science 2000, 35, 1205 – 1211.

61. Singh, K. B.; Bhosale, L. R.; Tirumkudulu, M. S., Cracking in drying colloidal films of flocculated dispersions. Langmuir 2009, 25, (8), 4284-7.

62. Park, J.; Willenbacher, N.; Ahn, K. H., How the interaction between styrene-butadiene-rubber (SBR) binder and a secondary fluid affects the rheology, microstructure and adhesive properties of capillary-suspension-type graphite slurries used for Li-ion battery anodes. Colloids and Surfaces A: Physicochemical and Engineering Aspects 2019, 579.

63. Toubal, L.; Karama, M.; Lorrain, B., Stress concentration in a circular hole in composite plate. Composite Structures 2005, 68, (1), 31-36.

64. Koo, M.; Park, K. I.; Lee, S. H.; Suh, M.; Jeon, D. Y.; Choi, J. W.; Kang, K.; Lee, K. J., Bendable inorganic thin-film battery for fully flexible electronic systems. Nano Letters 2012, 12, (9), 4810-6.

65. Kim, J. S.; Ko, D.; Yoo, D. J.; Jung, D. S.; Yavuz, C. T.; Kim, N. I.; Choi, I. S.; Song, J. Y.; Choi, J. W., A half millimeter thick coplanar flexible battery with wireless recharging capability. Nano Letters 2015, 15, (4), 2350-7.

66. Park, S.; Park, H.; Seong, S.; Chung, Y., Multilayer Substrate to Use Brittle Materials in Flexible Electronics. Scientific Reports 2020, 10, (1), 7660.

국문초록

본 연구에서는 모세관 현탁액을 이용한 리튬 이온 배터리 수계 음극 슬러리의 내부 구조 제어 및 이를 통한 전극의 기계적 물성 개선 방

안에 관해 고찰하였다.

모세관 현탁액(Capillary suspension)은 입자와 서로 섞이지 않는 두 유체인 벌크 유체와 2차 유체로 이루어 진 삼상계 시스템으로, 내부 구조와 흐름 특성이 일반 현탁액과 현저히 다른 특성을 보인다. 소량 첨가되는 2차 유체는 입자들 사이에서 모세관 힘을 일으키며 입자들을 잡아주는 역할을 하여 입자의 네트워크 구조를 형성시키고 흐름성을 변화시킨다. 이러한 특성들을 이용하여 Li-ion battery 전극 제조에 새로운 방향성을 제시하기 위하여 모세관 현탁액 개념을 battery 전극 슬러리에 적용하고, 이에 따른 내부 구조 변화 및 전극의 기계적 물성 변화에 대하여 알아보았다.

먼저, 모세관 현탁액 기반 전극 슬러리의 내부 구조를 변화시켜 첨가제인 SBR 바인더의 분포를 조절하고, 이를 통하여 전극의 접착 특성을 증진시키는 연구를 진행하였다. 유변 물성, 계면 특성, 구조 분석 등을 통하여 SBR 바인더 입자들이 모세관 현탁액 내에서 벌크 유체와 2차 유체 사이의 계면에 위치함을 알아내었다. 계면에 위치하는 SBR 바인더 입자는 모세관 현탁액의 흐름 특성을 변화시키는 역할을 하게 되며, 이는 믹싱 에너지에 따라 달라진다는 것도 확인하였다. 모세관 현탁액 기반의 전극의 경우 전극의 접착력에 관여하는 SBR 바인더의 분포 변화로 일반 전극 대비 접착 특성이 증진되는 경향을 보였다. 모세관 현탁액을 이용하여 바인더의 분포를 조정함으로써 전극의 접착력을 증진시키는 방안을 제시한 것이다.

다음으로, 모세관 현탁액 기반 전극 슬러리의 건조 중 특성 및 건조

후 내부 구조 관찰을 통하여 전극의 기계적 물성이나 안정성이 어떻게 변화하는지 알아보았다. 액상 구조 분석 및 FT-IR 등을 통하여 모세관 현탁액 전극 슬러리의 2차 유체는 건조 과정의 마지막 단계까지 남아 입자의 네트워크 구조를 유지시켜 주는 역할을 한다는 것을 확인하였다. 이로 인하여 모세관 현탁액 전극의 건조 후 공극률이 일반 전극 대비 증가하였고, 건조 후 잔여 스트레스는 감소하였다. 이러한 양상은 건조 후 전극의 안정성을 높여주는 효과를 주어, 외력에 의한 변형이 연속적으로 가해진 후에도 전극이 파괴되지 않고 기능이 유지되는 것을 확인할 수 있었다. 모세관 현탁액의 액상에서의 구조가 건조 중, 그리고 건조 후에 어떠한 영향을 미치며 건조 후 전극의 안정성에 어떻게 기여하는지 보여준 것이다.

본 연구를 통해 배터리 전극 슬러리의 내부 구조를 조절하고 이를 통하여 전극의 접착력 및 안정성을 증진시킬 수 있는 방안을 제시하였다. 다양한 기계적 물성의 보완이 요구되는 차세대 배터리 제작 기술에 기여할 수 있을 것으로 기대된다.

주요어: 배터리 슬러리, 모세관 현탁액, 미세 구조, 입자 네트워크, 접착 특성, 건조

학번: 2017-38662